Hindsight in 2020: Modeling Preventative Measures for Select Diseases in Ontario using Probabilistic Dynamic Programming and SEIR Compartmental Frameworks

by Lia Humphrey

A Thesis
presented to
The University of Guelph

In partial fulfilment of requirements
for the degree of

Master of Science
in
Mathematics & Statistics

Guelph, Ontario, Canada

ABSTRACT

HINDSIGHT IN 2020: MODELING PREVENTATIVE MEASURES FOR SELECT DISEASES IN ONTARIO USING PROBABILISTIC DYNAMIC PROGRAMMING AND SEIR COMPARTMENTAL FRAMEWORKS

Lia Humphrey
University of Guelph, 2021

Advisor(s):
Dr. Monica-Gabriela Cojocaru
Dr. Edward Thommes

In this work, we provide a "rear-view mirror" analysis for approaches to two different diseases that were relevant to Ontario in 2020. Using probabilistic dynamic programming, we simulate two versions of an optimized publicly funded shingles vaccination program for seniors; the first using existing vaccination data under the 2016-2019 program, and the second by building on a population with existing coverage and a new vaccine with improved efficacy. Then, using an SEIR compartmental model with ordinary differential equations, we use a derivative-free optimization method to model age-stratified case development of COVID-19 during the first wave of the pandemic, as well as determining the relative significance of specific NPI measures in slowing transmission. Lessons learned from the early handling of these diseases may inform better healthcare planning and prevent unnecessary future costs and suffering.

ACKNOWLEDGEMENTS

I would first like to thank my advisors, Dr. Monica Cojocaru and Dr. Ed Thommes, for their friendly expertise, guidance, and feedback during my research process. I'm continually grateful for the chance they took on an interdisciplinary student and the many opportunities afforded to me during our time together.

I am also indebted to my research partners for their valuable insight and contributions to this work. I am particularly grateful to Roie Fields, whose identical class schedule and extensive collaboration sessions greatly shaped my graduate experience.

I thank my parents and friends for their support and encouragement, as well as the various media platforms that allowed me to stay in touch despite the developing pandemic.

Finally, I honour each of my grandparents, whose pride and financial backing helped enable me to reach this academic milestone. I hope to honour their legacies in this work and that which follows.

TABLE OF CONTENTS

Abstract ii

Acknowledgements iii

Table of Contents v

List of Tables vi

List of Figures ix

List of Appendices x

1 Introduction 1

2 A model of vaccine distribution under a single-payer program umbrella: evaluating public shingles vaccine programs for seniors in Ontario, Canada 4
- 2.1 Introduction . . . 5
- 2.2 Methods . . . 8
- 2.3 Case Study: Addressing herpes zoster in Ontario . . . 12
  - 2.3.1 Estimating Uptake and Population Coverage . . . 13
  - 2.3.2 Ontario distribution of Zostavax: 2016-2020 . . . 15
  - 2.3.3 Ontario distribution of Shingrix: 2020 and beyond . . . 20
- 2.4 Discussion . . . 23
  - 2.4.1 Program impacts . . . 23
  - 2.4.2 Comparison to other HZ immunization programs . . . 30
  - 2.4.3 Assumptions . . . 31
- 2.5 Conclusion and future work . . . 32

3 Age-stratified transmission model of COVID-19 in Ontario, Canada with human mobility during pandemic's first wave 34
- 3.1 Introduction . . . 35
  - 3.1.1 Background . . . 36
- 3.2 Methods . . . 40

3.2.1 Adapted SEIR model . . . 40
3.2.2 Ontario specific parameter values and data sources . . . 43
3.2.3 Deriving contact rates for Ontario pre-pandemic . . . 44
3.2.4 Case onset and mobility data . . . 46
3.2.5 Dampening contact rates to replicate behavioural changes and preventative measures . . . 48
3.2.6 SEILR(pas) model results . . . 53
3.3 Results & Discussion . . . 55
3.3.1 Removing outbreaks to match age-specific case rates . . . 55
3.3.2 Estimates of mobility and behaviour during the pandemic's first wave 57
3.4 Limitations and further work . . . 64
3.5 Conclusion . . . 65

4 Concluding remarks 67

References 69

Appendices 79

LIST OF TABLES

2.1 Parameters and variables of the PDP problem. 10
2.2 Calculation for the expected monthly vaccine coverage in group i for distribution amounts up to demand $x_i(t)$. 11
2.3 Calculation for the optimal allocation of vaccines that attains the maximum expected coverage in our objective function. 12
2.4 Year-specific distributions of Zostavax at two price points. 17
2.5 Year-specific distributions of Shingrix at two price points. 23

3.1 Parameters and initial values of the SEILR system (3.2.1). 44
3.2 Contact rates calculated for the three Ontario population subgroups. Contact rates are taken from Canadian estimates by [86] and weighted according to census data from Statistics Canada [108]. 50

A.1 Population numbers for 65-69 year olds from 2016-2020, taken from yearly provincial estimates [123]. 80
A.2 Population numbers for 65-69 year olds in 2021-2024 are projections from 2020 population estimates for 61-64 year olds using average Ontario growth rate trends for seniors from the last decade [123]. 81
A.3 Model results for doses administered and effective coverage with Zostavax in 2020 by age. 81
A.4 Model results for doses administered and effective coverage with Shingrix in 2024 by age. 81

LIST OF FIGURES

2.1 Percentage of individuals by age year who received Zostavax doses between 2016-2020, compared with resulting coverage levels in 2020 (price = $200). The five rightmost age groups represent those who were between 65-69 in 2016. The shaded region indicates the most recent cohort of 65-69 year olds vaccinated in 2020. 18
2.2 Percentage of individuals by age year who received Zostavax doses between 2016-2020, compared with resulting coverage levels in 2020 (price = $100). The five rightmost age groups represent those who were between 65-69 in 2016. The shaded region indicates the most recent cohort of 65-69 year olds vaccinated in 2020. 19
2.3 Total number of Zostavax doses allocated each year by age, 2016-2020 (price = $100). Vaccine allocation breakdown for all Ontarians who were age-eligible at some point for Ontario's publicly funded HZ immunization program between 2016-2020, assuming a 50% manufacturer's price discount. Note: exact group allocations may vary slightly between simulations each year due to the random order of group arrival in the DP distribution process, but yearly distributed totals remain the same. 21
2.4 Percentage of individuals by age year who received Shingrix courses between 2020-2024, compared with resulting coverage levels in 2024 (price = $300). The five rightmost age groups represent those who were between 65-69 in 2020. The shaded region indicates the cohort of 65-69 year olds vaccinated in 2024. 24
2.5 Percentage of individuals by age year who received Shingrix courses between 2020-2024, compared with resulting coverage levels in 2024 (price = $150). The five rightmost age groups represent those who were between 65-69 in 2020. The shaded region indicates the cohort of 65-69 year olds vaccinated in 2024. 25

2.6 Total number of Shingrix courses allocated each year by age, 2020-2024 (price = $150). Vaccine allocation breakdown for all Ontarians who are age-eligible at some point for Ontario's publicly funded HZ immunization program between 2020-2024 (excluding those who had already received Zostavax), assuming a 50% manufacturer's price discount. Note: exact group allocations may vary slightly between simulations each year due to the random order of group arrival in the DP distribution process, but yearly distributed totals remain the same. 26
2.7 Comparison of coverage (effective protection) conferred to those vaccinated with Zostavax between 2016-2020 versus Shingrix between 2020-2024. When compared over respective 50 month periods for each program, Shingrix clearly offers superior protection until the program runs out of doses. 28
2.8 Population coverage (effective protection) in 2024 for recipients of Zostavax (price = $100) from 2016-2020 versus Shingrix (price = $150) from 2020-2024. Note that Zostavax's efficacy beyond 5 years since vaccination is not well documented, so the protection rate for anyone who received Zostavax earlier than 2020 is fixed at the Year 5 rate (14%) [35]. Thus, Zostavax's contribution to protection levels in 2024 are likely lower in reality than shown here. 29

3.1 Schematic of SEILR(pas) model for COVID-19 progression and control measures for a Group i, $i \in \{1, 2, 3\}$. The outward arrow labelled β_{ij} implies that the encircled compartments (Presymptomatic, Asymptomatic, and Symptomatic infected) in each age group have an impact on new transmissions to the other age groups $\{1, \ldots, 3\}$. 41
3.2 iPHIS data (black) and simulated pre-lockdown symptomatic infections in each of the 3 groups. The blue curve represents symptomatic infected in the overall Ontario population. 50
3.3 Simulated new daily symptomatic infections in each of the 3 age groups according to the SEILR(pas) model. 51
3.4 Simulated new daily symptomatic infections in each of the 3 age groups compared with iPHIS reported cases, stratified by age. 54
3.5 Proportion of COVID-19 cases in Ontario attributed to each age group for the real iPHIS reported numbers (top; total = 32,095, Group 1 = 1,336, Group 2 = 18,595, Group 3 = 12,004) vs. the SEILR(pas) model (bottom; total = 31,722, Group 1 = 1,029, Group 2 = 22,407, Group 3 = 8,286). 54
3.6 Simulated new daily symptomatic infections in each of the 3 age groups compared with iPHIS reported cases, stratified by age, **with outbreaks removed**. 56

3.7 Proportion of COVID-19 cases in Ontario attributed to each age group **with outbreaks removed** for the real iPHIS reported numbers (top; total = 18,614, Group 1 = 1,222, Group 2 = 12,985, Group 3 = 4,407) vs. the SEILR(pas) model (bottom; total = 17,970, Group 1 = 582, Group 2 = 12,705, Group 3 = 4,683). 57
3.8 Change in q over time as compared to threshold, $\bar{q} = 0.17$. 59
3.9 Comparison of SEILR(pas) model epidemic curves, with and without mobility data. 60
3.10 Relative changes in mobility data, the transmission scaling factor (q), and the the transmission scaling factor decoupled from mobility data ($\hat{q}$) from February 14 - June 7. 61
3.11 Change in q over time with outbreak cases removed as compared to threshold $\bar{q} = 0.17$. 63

B.1 To solve for the q value for time interval int (between the two black lines), we find the SSE during time interval $int + 2$ (red shaded region). 85

LIST OF APPENDICES

Appendices 79

A Supplementary data for shingles distribution model 80
A.1 Population estimates 80
A.2 Age group-specific distribution results 80

B Supplementary calculations for SEILR(pas) model 82
B.1 Collapsing age-stratified contact matrices 82
B.2 Initial start date 83
B.3 Matching the delay between simulated data and iPHIS data 83

Chapter 1

Introduction

Over the past year, the public health domain grappled with many challenges and lessons. COVID-19 undoubtedly took center stage as concerns for resource allocation, medical infrastructure, and public cooperation became ubiquitous in day-to-day life. However, in the background, similar themes arose for the management of other diseases, for which investigation was less pressing but nevertheless relevant. Whether the pressure is immediate or insidious, initial responses may provide telling insight as to how current strategies or future developments may ultimately play out. As such, we match to Ontario data sets in two different models to explore and optimize trends defining the progression and responses to COVID-19, an infectious disease, and herpes zoster (shingles), a non-infectious disease, which were provincially relevant in 2020.

We begin with shingles, a non-life threatening disease that will affect approximately 1 in 3 Canadians in their lifetime, mainly those over the age of 50 [1]. While non-lethal, shingles inflicts serious impairment on quality-of-life that can become permanent, costing millions per year in hospital and treatment-related costs. Ontario spends almost half of its healthcare resources on seniors (age 65+), who currently make up less than 20% of the population but are the fastest growing category [2]. As of 2017, there are only two shingles vaccines authorized for use in Canada. Since shingles is predominantly a disease of older adults, Ontario launched a pilot program to publicly fund immunization for 65-69 year olds

from 2016-2020 with Zostavax (Merck Frosst Canada Ltd.) [3], and released an update to the program in 2020 replacing Zostavax with Shingrix (GlaxoSmithKline Inc.) [4]. At the time of writing, no data on either version of the program is publicly available, and to date, Ontario does not coordinate a consistent immunization registry across its public health units, often relying on provincial surveys for coverage information as opposed to data from the healthcare providers who administer the vaccines [5]. Furthermore, vaccination data for HZ has only been surveyed in Ontario biannually since 2016 [6]. Differences in efficacy between the two vaccines raise questions as to how many people received the first vaccine, and whether it would be ethical and/or cost-effective to supplement their immunity through inclusion in the newer program. We simulate current potential shingles protection levels in the population using a probabilistic dynamic programming framework with a Poisson-distributed arrival process, and use these estimates to forecast costs and immunity levels for the newer program.

We then transition to studying Ontario's early pandemic response to COVID-19 beginning in March, 2020, which consisted of non-pharmaceutical interventions (NPIs) including physical distancing, mask-wearing, and shelter-in-place orders. We employ a tailored SEIR compartmental model and a derivative-free optimization method to match to accurate episode date data provided by the province's public health units (PHUs) to estimate the impact of these NPIs. We do so by stratifying the population into three subcategories and applying heterogeneous contact and asymptomatic rates, as well as comparing the inclusion and exclusion of local outbreak clusters to refine our results. Further, we quantify the confounding effects of individual mobility on transmission to decouple the impact of sheltering in place versus other NPIs. Our period of study ranges from the first government restrictions to the start of more widespread community testing (March - June, 2020) as cases from this time period represent solely NPI preventative policies. We then compare to pre-lockdown behaviour in the month leading up to restrictions. The structure of this thesis will begin

with two chapters presenting the disease frameworks mentioned here, followed by concluding remarks and supplementary data provided in the appendices.

Chapter 2

A model of vaccine distribution under a single-payer program umbrella: evaluating public shingles vaccine programs for seniors in Ontario, Canada

Abstract

In this work, we develop a probabilistic dynamic programming framework to optimize distribution of vaccines in a multi-year immunization program for a non-infectious disease. We apply this model to a case study of herpes zoster (shingles) in Ontario, estimating population protection levels in 65-69 year olds under a publicly funded vaccination program established from 2016-2020. We then build on these findings to make comparable coverage predictions for Ontario's second iteration of the program using a newer, more effective vaccine. We compare

our results in each program to those of shingles immunization programs in other countries and highlight considerations for program design for optimal uptake and social benefit.

2.1 Introduction

Public health systems and research face many challenging situations when it comes to addressing the myriad complexities that constitute human vitality. For example, since December 2019, the novel coronavirus SARS-CoV-2 has served as an alarming reminder that new and existing diseases occur among populations for which treatments, prophylactics, and public health programs do not yet exist. Vaccines, once available, are a preferred tool for the prevention of illness, disability, and death, because when administered effectively, vaccines are highly cost-effective by decreasing or eliminating the larger and longer-term costs a health system may spend on clinical care (e.g. antiviral therapy, physician visits, hospitalizations) [7]. Timelines to develop a solution such as a vaccine may vary by urgency, but the resulting situation remains the same —deciding how to best allocate (scarce) resources when data is sparse, uncertain, or non-existent.

Herpes zoster (shingles, or HZ) is an example of a well-studied disease which only recently became authorized as vaccine-preventable for Canadians in 2011 [8]. Until 2016, the vaccine Zostavax was only available to individuals privately, but the lack of a consistent immunization tracking system among all provinces and territories meant relatively meager data for public uptake and demand. Ontario became the first province to pilot a publicly funded vaccination program with Zostavax for seniors in the 65-69 year old age bracket from 2016-2020, and recently adopted and upgraded the program to offer the newer, pricier, and more effective competitor Shingrix in 2020.

Total costs and effectiveness for protecting the target population have not been publicly released for either program. In this work we investigate several fundamental questions: 1)

how the Zostavax distribution schedule may have proceeded in 2016-2020 in order to match up to available aggregate demand data; 2) the level of shingles protection that exists to date for the age brackets that were covered under this program; 3) scenario-testing of the new permanently adopted vaccine schedule with Shingrix and the evolution of shingles coverage in the next 3-4 years in Ontario.

To answer the first question, we employ a resource allocation model based on a probabilistic dynamic programming (DP) model. DP offers one method for determining resource distribution to different groups based on various constraints, particularly when resource quantities must be measured in whole numbers (e.g. people, vaccine doses), and when future circumstances/demand are unknown. By developing a DP model to quantify optimal coverage estimates for shingles from 2016 onwards, we provide a framework that may be useful to other regions and provinces in developing an immunization program that respects a given budget and maximizes the subsequent effects on patients' quality of life. As a case study, we apply our DP model to the specific case of shingles vaccination in Ontario to analyze its publicly funded shingles immunization program.

The DP method has a history of use in the biological sciences since its inception by Richard Bellman in the 1950s [9], applied to reduce inefficiencies in healthcare operations such as patient procedure scheduling, hospital bed allocation, and resource production/-supply chains (see for example, [10, 11, 12]). DP has also been used to solve vaccination distribution problems in various contexts. Hethcote & Waltman (1973) investigated vaccination schedules via DP in a deterministic differential SIRV model to minimize program costs for preventing simulated theoretical epidemics [13]. However, the parameters of disease dynamics are rarely known with certainty. Tanner, Sattenspiel, and Ntaimo (2008) refined the cost-minimizing epidemic prevention problem exemplified in [13] using stochastic DP to incorporate probability distributions for unknown inputs [14]. Furthermore, influenza vaccination programs, widely studied in mathematical epidemiology, face a number of annual

logistical uncertainties that have been addressed with stochastic DP frameworks: Ozaltin et al. (2018) explored the dynamic composition and production timing of yearly flu vaccines in a multistage stochastic mixed-integer program to quantify costs and benefits to various policy designs [15]. Wu, Wein, & Perelson (2005) investigated the impact of repeated influenza vaccination, which may actually decrease vaccine efficacy according to an individual's previous strain exposure. A stochastic DP is used to compare effective flu shot protection when production for future strains are based on surveillance data versus the population's antigenetic history [16]. Harvey et al. (2018) specifically studied a cost-effective vaccination strategy for herpes zoster (HZ) using stochastic DP, which evaluated whether to vaccinate an individual at a given age with Zostavax or defer vaccination for a year based on sex, age, HZ vaccine efficacy, risk likelihood, and resulting burden of illness (BOI) when not receiving a vaccine [17].

Publicly funded vaccination programs for HZ, a non-infectious disease, in both England [18, 19] and Australia [20] have proven to reduce the number of HZ cases in their respective populations (70 years olds with catch-up for 71-79 year olds). In each case, vaccine uptake and coverage were estimated by extracting data from primary care networks and performing regressions to determine approximate cases prevented and vaccine effectiveness in that age group. Both programs were conducted using Zostavax, and each study concluded that overall uptake and protection in the programs are suboptimal in terms of total cost-effectiveness and social benefit. However, at the time of writing, England and Australia have yet to adopt Shingrix in their programs, meaning that protection estimates with Shingrix in Ontario, coupled with existing coverage estimates under Zostavax, may provide valuable insight into the viability of similar program upgrades to achieve the original goals of cost-minimization and shingles protection. Without similar primary care dataset access, here we present a multistage probabilistic DP model for a non-infectious disease in hopes of maximizing population protection under a fixed budget.

The structure of the paper is as follows. In Section 2.2, we establish the definitions and methodology of our probabilistic DP problem to maximize vaccine protection for given population subgroups. In Section 2.3, we apply our model as a case study for publicly funded HZ vaccination in Ontario, Canada, and estimate current and future population protection for two different vaccines. In Section 2.4, we compare and contrast the performance of the two vaccines against each other, and then against HZ vaccination policies in other parts of the world. Finally, we summarize our findings and provide extensions for future work in Section 2.5.

2.2 Methods

Our model computes maximal vaccine coverage for a general vaccination program, taking into account the efficacy of the vaccine and a probabilistic vaccine uptake estimate. We define "coverage" (or "effective protection level") to mean the percentage of a vaccinated population that has adequate immunity to the disease, according to the efficacy of a given vaccine. Using a first-come-first-served queue model of vaccine demand among different age groups, we use a multistage probabilistic dynamic programming (PDP) approach to optimize the program's vaccine coverage under a fixed budget. Furthermore, we apply our model repeatedly over a long time span that generally represents several years of physical time, with a time-step unit of 1 month. We consider a number of senior population subgroups divided by 1-year age increments, and denoted by $i \in \{1, 2, ..., n\}$, with respective sizes denoted by G_i. We consider that there is a total budget for the program in a single-payer health system, denoted by B, and we assume the price per treatment is denoted by p. $x_i \in \mathbb{Z}_+$ represent a possible vaccine allocation value to group i, and 1 unit of allocation is considered to be equivalent to 250 real life vaccine courses. This conversion was determined via sensitivity analysis that considered both the total average monthly demand based on our arrival rates and the simplification

of calculations. We use a simple Poisson arrival process to express the likely number N_t of seniors in group i that demand to be vaccinated in a unit time t, assuming average arrival rates λ_i calculated for each group i. This probability is given by

$$P_i(N_t = x_i, \lambda_i) = \frac{e^{-\lambda_i t}(\lambda_i t)^{x_i}}{x_i!}, \text{ with } x_i \in \mathbb{Z}_+ \text{ as described above.}$$

The vaccine coverage function we evaluate in each time unit t is:

$$f_i(x_1(t), x_2(t), ..., x_i(t)) = \sum_{i=1}^{n} x_i(t)\, e_i\, P_i(x_i(t), \lambda_i(t))$$

subject to $\sum_{i=1}^{n} p x_i(t) \leq B_t$ and $x_i(t) \in \mathbb{Z}_+$, with B_t representing a budget per unit time t. Then our multi-year vaccine coverage problem to solve is:

$$\begin{aligned} \max \quad & \sum_{t} f_i(x_1(t), ..., x_i(t)) \\ \text{s. t.} \quad & \sum_{t} (\sum_{i=1}^{n} p x_i(t)) \leq \sum_{t} B_t = B \\ & x_i(t) \in \mathbb{Z}_+, \forall t \end{aligned}$$

This is an integer optimization problem with a nonlinear objective function subject to linear constraints, where the stages are the population subgroups, the states are the number of vaccines assigned to a subgroup (based on vaccine efficacy and probability of demand for that number of vaccines), and the return is the effective population protection conferred by vaccination. A summary of the symbols and notation used in this paper are provided in Table 3.1. Due to the need to solve for values of allocation vectors x in the set of non-negative integers, we proceed to apply a probabilistic dynamic programming (PDP) framework to obtain our optimal allocation levels.

In our model, vaccine inventory numbers, arrival rates, overall budget, length of program,

Table 2.1: Parameters and variables of the PDP problem.

Symbol	Definition
G_i	Size of population subgroup $i \in \{1, 2, ..., n\}$
B	Total budget for the program
B_t	Estimated budget per unit time t
p	Price of a vaccine
e_i	Efficacy of vaccine in group i
$X = \frac{B_t}{p}$	Maximum number of vaccines available to all groups in one time unit
x_i	Allocation to group i, per unit time t, $0 \leq x_i \leq X$
λ_i	Expected arrival rate (mean number of seniors requesting vaccination from i per unit time t)
$P(x_i, \lambda_i)$	Estimated demand for an allocation x of vaccine in group i per unit time

and senior group sizes are known. The optimal allocation of vaccines to groups, the overall coverage at end of program and the program cost are evaluated/computed at each stage of the PDP process. In general, PDP begins by solving the last stage problem, then progressing backwards through all previous stages $\{n-1, n-2, ..., 2, 1\}$. In our case, we cannot a priori determine the last stage of our problem, as that would imply an order in the incoming vaccination requests from the n subgroups. This would be inconsistent with how the process unfolds in reality, therefore we shuffle the distribution order of the subgroups at every time step allocation, and run a large set of simulations to ensure that reordering the stages does not affect our optimal allocation results. Furthermore, optimization problems are generally static, but our model incorporates time-dependency as we are considering repeated iterations of our objective function over multiple months. Thus, for each time unit t, let us describe the PDP formulation of our problem, consistent with the description of our stages $\{1, 2, \cdots, n\}$:

For each group i, define $r_i(x_i(t)) := x_i(t)e_iP(x_i(t), \lambda_i(t))$ to be the expected vaccine coverage from a number of x_i doses assigned to group i per time unit t.

For each group i, let $f_i(x_i(t))$ be the maximum expected vaccine coverage achieved from distributing x_i doses to the groups $\{i, i+1, i+2, \cdots, n\}$ per time unit t. Stage n:

$$f_n(x_n(t)) = \max_{x_n(t)} \; r_n(x_n(t)) = \max_{x_n(t)} \; x_n(t)e_nP_n(x_n(t), \lambda_n(t)), \quad \text{s.t.} \quad 0 \leq x_n(t) \leq X,\, x_n(t) \in \mathbb{Z}_+$$

Stage $i < n$:

$$f_i(x_i(t)) = \max_{g_i}\{r_i(g_i) + f_{i+1}(x_i(t) - g_i)\}, \quad \text{s.t.} \quad \begin{cases} 0 \leq g_i \leq x_i(t), \\ 0 \leq x_i(t) \leq X,\, x_i(t) \in \mathbb{Z}_+, \\ \sum_{i=1}^{n} p x_i(t) \leq B_t \end{cases}$$

In Tables 2.2 and 2.3 we describe in detail the computation of the expected vaccination coverage functions from the definitions above. This DP formulation is similar to the classic inventory distribution problem with future state certainty but current reward uncertainty in Chapter 19 of [21].

Table 2.2: Calculation for the expected monthly vaccine coverage in group i for distribution amounts up to demand $x_i(t)$.

Group i	Distribution levels $0 \leq g_i \leq x_i(t)$	Expected Vacc. Cov. $r_i(g_i)$
	$g_i = 0$	$0 \cdot e_iP(0, \lambda_i(t)) = 0$
	$g_i = 1$	$e_iP(1, \lambda_i(t))$
	$\cdots$	$\cdots$
	$g_i = x_i(t)$	$x_i(t)e_iP(x_i(t), \lambda_i(t))$

Table 2.3: Calculation for the optimal allocation of vaccines that attains the maximum expected coverage in our objective function.

Group $i < n$	Distribution levels $0 \leq g_i \leq x_i(t)$	Monthly demand level $x_i(t)$	Max. Expected Coverage $f_i(x_i(t))$
	$g_i = 0$	0	$r_i(0) + f_{i+1}(0-0)$
	$g_i = 0$ $g_i = 1$	1	$\max \begin{cases} r_i(0) + f_{i+1}(1-0) \\ r_i(1) + f_{i+1}(1-1) \end{cases}$
	$g_i = 0$ $g_i = 1$ $g_i = 2$	2	$\max \begin{cases} r_i(0) + f_{i+1}(2-0) \\ r_i(1) + f_{i+1}(2-1) \\ r_i(2) + f_{i+1}(2-2) \end{cases}$
	$\cdots$	...	...
	$g_i = 0$ $g_i = 1$ $\cdots$ $g_i = X$	X	$\max \begin{cases} r_i(0) + f_{i+1}(X-0) \\ r_i(1) + f_{i+1}(X-1) \\ \cdots \\ r_i(X) + f_{i+1}(X-X) \end{cases}$

2.3 Case Study: Addressing herpes zoster in Ontario

Herpes zoster (shingles) is a debilitating neurocutaneous disease that will affect approximately 1 in 3 Canadians in their lifetime [22, 23]. Shingles results from the reactivation of the varicella-zoster virus (VZV, or chickenpox), meaning nearly 90% of adults are at risk for developing shingles and further complications [24, 25]. For a person seropositive for VZV, age is the main determinant of infection risk, with substantial increases beyond 50 years of age due to immunosenesence [26]. One of the biggest concerns associated with shingles is the development of a more serious degenerative condition called post-herpetic neuralgia (PHN), a severe pain condition affecting up to 30% of shingles patients that persists anywhere from three months to several years and often requires hospitalization [27, 28, 29]. A Manitoba study estimated an average HZ case costing $401 (incorporating physician visit fees and antiviral drug prescriptions) and $12,000 for more serious cases requiring hospitalization [1]. Around 130,000 new cases of shingles occur annually in Canada, totalling approximately $67

million in annual healthcare costs ($73 million in 2020) [30, 5].

2.3.1 Estimating Uptake and Population Coverage

In October 2017, Canada became the first country to authorize use of two different HZ vaccines by approving the recombinant subunit vaccine Shingrix [31]. Compared to Zostavax, Shingrix has a higher market price (approx. $200 vs. $300 CAD, respectively) but a significantly higher protection rate and duration against HZ in all age groups (peak protection rates at 64% vs. 97%) [23]. Since 2018, the National Advisory Committee on Immunization (NACI) has recommended Shingrix as the federal standard of care for preventing shingles over Zostavax. Both of these changes occurred in the midst of Ontario's first publicly funded HZ vaccination program, which launched in September 2016 and committed $68 million over three years to provide Zostavax to people aged 65-69 (among the most cost-effective age groups for Zostavax) [23, 32]. Effective October 2020, Ontario updated its program to replace Zostavax with Shingrix for an unspecified duration and yearly cost [33].

We wish to study the long-term costs and benefits of publicly funding the Shingrix vaccine for this age group, which may be applicable not only to provinces without such a policy, but also to other age cohorts within Ontario. However, unlike other publicly-funded vaccines in Canada's recommended adult immunization schedule (influenza, pertussis, diptheria & tetanus, pneumococcal), HZ vaccine coverage has been minimally surveyed [23], and data from the pilot program, including overall costs, population demand and coverage, and program cost-effectiveness are not publicly available. As a result, these parameters must be estimated in order to evaluate the impact of each program.

Between 2008-2016, it is known that 20.4% of Canadians aged ≥ 50 years (denoted by CAN_{50+}) received Zostavax in total [23]. Since there was no program anywhere in Canada

for HZ at that time, it is reasonable to assume no difference in demand in Ontarians over 50. Therefore our starting point is

$$CAN_{50+} = 20.4\% = ON_{50+} + RC_{50+},$$

where ON_{50+} denotes the number of Ontarians aged ≥ 50 and RC_{50+} denotes the number of people aged ≥ 50 in the rest of Canada (RC). By 2018, things are more interesting. We assume that without the program, vaccination rates would have continued to grow at a rate of (20.4% / 8 years) = 2.55% per year, resulting in CAN_{50+} = (20.4%) + (2 years $\times$ 2.55%) = 25.5% total. However, Canada's 2018 overall HZ vaccination level was 28% [34]. Since Ontario was the first and only province offering HZ vaccination for free between 2016-2018, we assume this increase beyond expected growth is due to higher vaccination rates in Ontario, while the rest of CAN_{50+} continued to get vaccinated at trend level. The 2018 allocation level in the CAN_{50+} population is now given by:

$$28\% = x\%(\frac{ON_{50+}}{CAN_{50+}}) + 25.5\%(\frac{RC_{50+}}{CAN_{50+}})$$

Plugging in these known population numbers for Ontario and Canada, we solve for x = 32.03% of ON_{50+} (1,732,057 people) vaccinated with Zostavax between 2016-2018. Furthermore, since the ON program only included the ages $65-69$ (denoted by ON_{65-69}), we can further refine our computation to deduce the respective weight of vaccination attributable to the existence of the program in ON:

$$x\% = 25.5\%(\frac{ON_{not-in-program}}{ON_{50+}}) + y\%(\frac{ON_{65-69}}{ON_{50+}})$$

Solving, we estimate y = 72.07% of Ontarians aged 65-69 (546,318 people) were vaccinated through the program in the first two years. This translates to a uniform monthly demand

of (72.07% / 24 months) = 3.003% per month. We implement this rate in our computation of the group arrival rates below.

2.3.2 Ontario distribution of Zostavax: 2016-2020

Now we apply our model using the assumptions in the previous section to illustrate optimal uptake for the Zostavax program; comparing results will help calibrate the model to predict program performance under Shingrix in the following section. Age group sizes for individuals aged 65-69 years from 2016-2020 are outlined in Table A.1, according to yearly population estimates. It is important to note that Zostavax efficacy is dependent upon age at vaccination and time since vaccination [31]. We assume that the initial Zostavax efficacy for 60-69 year olds (64%) applies to our age cohort, and that the coverage from one to five years post-vaccination decreases according to the estimates laid out in [35, 36]. Ontario promised a budget B = \$68 million for three years starting in September 2016 [32]. Given that no substitute program was announced between September 2019 and the introduction of the new program in October 2020, we include all of 2019 and 2020 in our calculation timeline in the case of left over doses or additional remaining funds. We investigate two pricing scenarios for Zostavax: 1) market price at p = \$200, and 2) a 50% reduction in market price (p = \$100) to simulate a potential government discount per dose. When p = \$200, we have 340,000 doses to distribute over 50 months (September 2016 to October 2020), and when p = \$100, we have 680,000 doses. Recall we assume that 1 unit of simulated treatment represents 250 vaccination courses in real life, and that the probability for group i to demand 250 units of treatment is equal to the probability that we serve up to 250 customers per month from group i. Uptake results from other publicly funded HZ vaccination programs (Australia, England) demonstrate that it is reasonable for demand to be significantly higher in the first years of the program compared to subsequent years, as the bulk of uptake happens when

individuals first become eligible [19, 20]. In lieu of most recent uptake data, we assume a similar drop rate in demand in 2019-2020 as in 2017-2018 ($\approx 50\%$ decrease per year). Our arrival rates are calculated as follows:

$$\lambda^t(2016) := 0.03003 \cdot \Big(G(2016)\Big),\ t = 1, \cdots, 4$$

$$\lambda^t(2017) := 0.03003 \cdot \Big(G(2017) - G^{vacc}(2016)\Big),\ t = 5, \cdots, 16$$

$$\lambda^t(2018) := 0.03003 \cdot \Big(G(2018) - \sum_{j \in \{2016,2017\}} G^{vacc}(j)\Big),\ t = 17, \cdots, 28$$

$$\lambda^t(2019) := 0.03003/2 \cdot \Big(G(2019) - \sum_{j \in \{2016:2018\}} G^{vacc}(j)\Big),\ t = 29, \cdots, 40$$

$$\lambda^t(2020) := 0.03003/4 \cdot \Big(G(2020) - \sum_{j \in \{2016:2019\}} G^{vacc}(j)\Big),\ t = 41, \cdots, 50,$$

where G is a vector of the sizes of groups in a given year, G^{vacc} represents previous years' vaccinated individuals who are removed from the remaining unvaccinated population, $t = 1$ represents September 2016, and $t = 50$ represents October 2020.

Using our model, when the price per dose is \$200, we estimate Ontario having administered all of its 340,000 potential vaccination treatments of Zostavax by May 2018, costing the entire budget of \$68 million (Figure 2.1). However, the provincial government may negotiate a contract with a discounted bulk price per unit from the vaccine manufacturer [37]. If we assume a 50% discount per treatment (p = \$100, doses available = 680,000), Ontario will have administered approximately 636,000 doses by the end of the original program in October 2020 (Figure 2.2). In terms of year-specific distribution, when p = \$200, we estimate 87,000 doses distributed in the last four months of 2016, 192,000 in 2017, and 61,000 in 2018. At p = \$100, distributions for 2016 and 2017 remain the same, followed by an allocation of 190,000 in 2018, 110,000 in 2019, and 57,000 in 2020.

Table 2.4: Year-specific distributions of Zostavax at two price points.

	$p = \$200$	$p = \$100$
2016	87,000	87,000
2017	192,000	192,000
2018	61,000	190,000
2019	0	110,000
2020	0	57,000
Total	340,000	636,000

Yearly program costs and distribution totals are highest under both pricing schemes in 2017, when demand is highest at 3.003% uniformly per month for 12 months. In both scenarios, our estimates for the total doses distributed over the first two years (assuming the inclusion of the last 4 months of 2016) are lower than the 546,318 doses predicted in the same time frame from population data alone. One factor explaining this could be higher demand in this period than estimated. The nature of our simulated arrival process is to compute and use the most likely level of doses demands by each subgroup per month, but in reality there may be month-to-month fluctuations where demand is higher than normal (e.g. seasonal influence, advertising, etc.). Additionally, arrival rates among the subgroups are unlikely to be uniform, as assumed here. It is possible that more demand is concentrated in the larger, younger age groups than being evenly distributed. Results from the upcoming 2021 edition of the adult National Immunization Coverage Survey (aNICS) may provide the modeller with more detailed demand data to assess both of these points.

For the remainder of this discussion, we assume the lower pricing scheme of $p = \$100$ for Zostavax, as this supplies sufficient doses to model potential outcomes in 2019 and 2020. Looking at the distribution of doses allocated over the course of the program in Figure 2.3, is obvious that 69 year olds (the 65 year old cohort in 2016) received the most doses of Zostavax (96.22% of their age group), as they had the longest period of eligibility of all

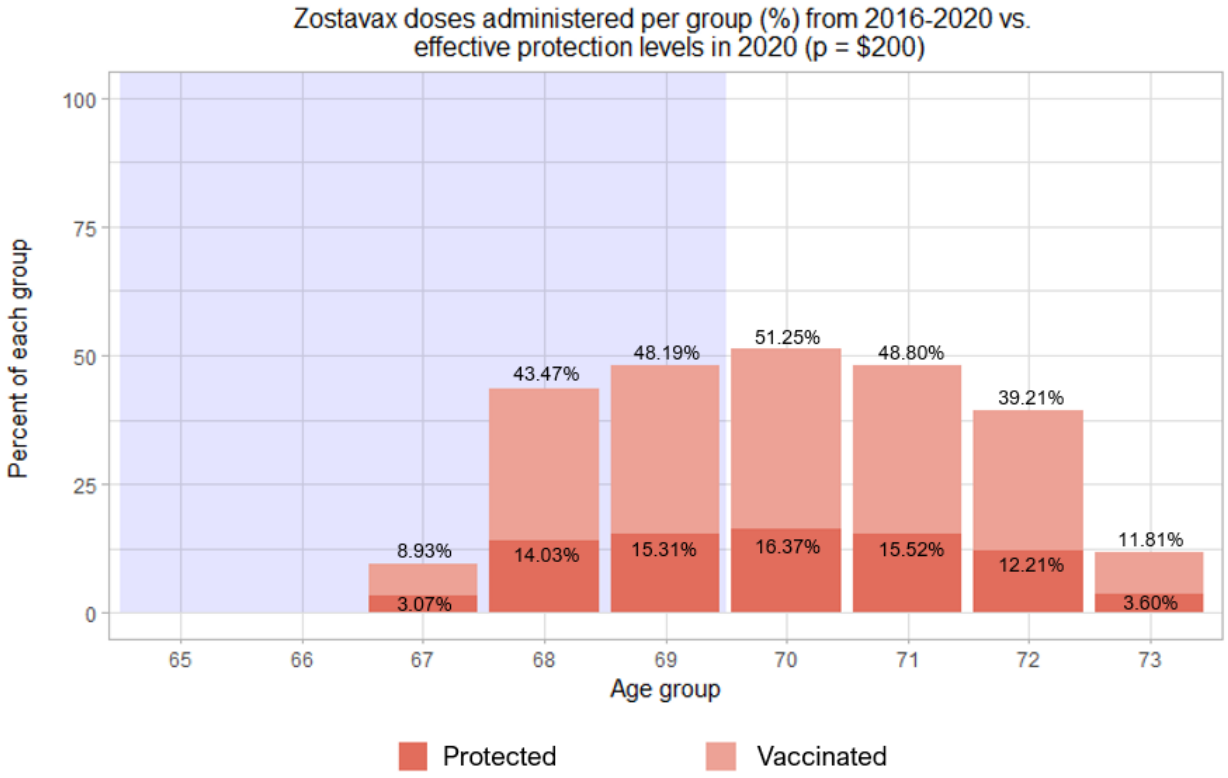

Figure 2.1: Percentage of individuals by age year who received Zostavax doses between 2016-2020, compared with resulting coverage levels in 2020 (price = $200). The five rightmost age groups represent those who were between 65-69 in 2016. The shaded region indicates the most recent cohort of 65-69 year olds vaccinated in 2020.

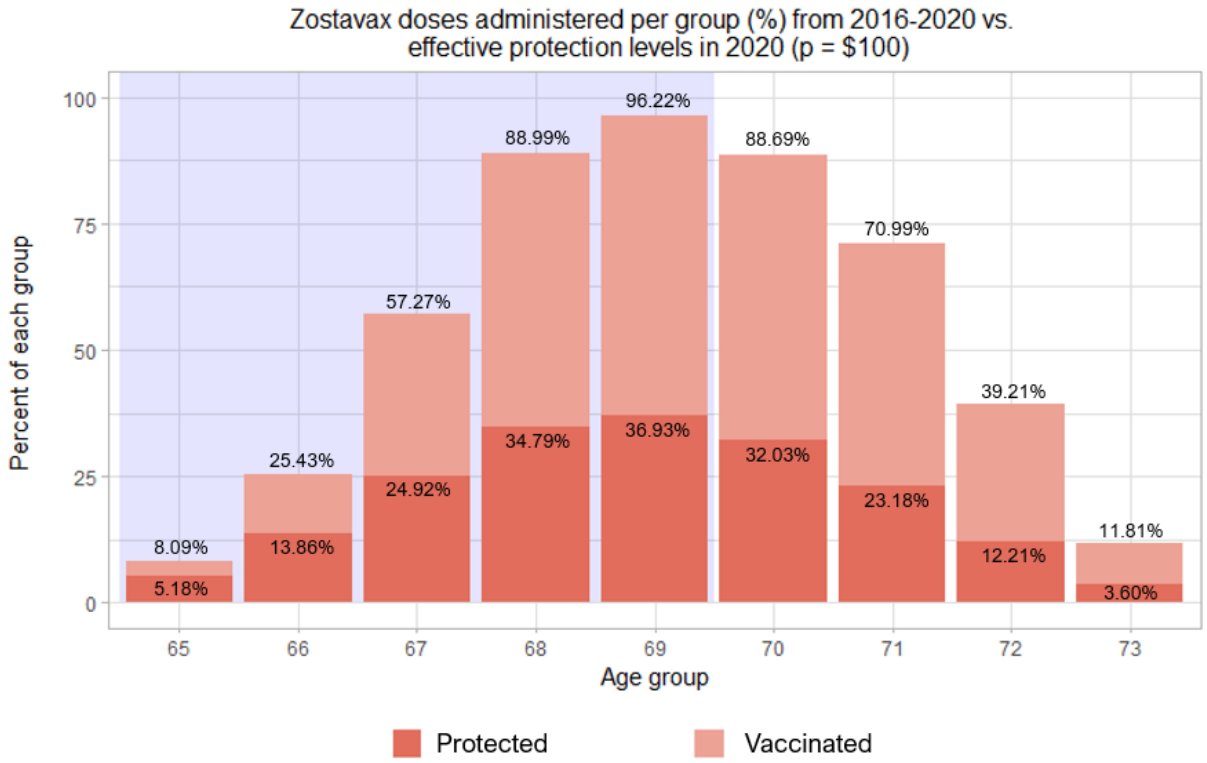

Figure 2.2: Percentage of individuals by age year who received Zostavax doses between 2016-2020, compared with resulting coverage levels in 2020 (price = $100). The five rightmost age groups represent those who were between 65-69 in 2016. The shaded region indicates the most recent cohort of 65-69 year olds vaccinated in 2020.

subgroups. Similarly, 65 year olds (61 year olds in 2016) received the lowest number of doses of the original cohort (8.09% of their age group), as their small period of eligibility was accompanied by the lowest yearly rate of demand. For the same reason, demand is highest in the first two years of the program and dwindles to a quarter of the original level by 2020, resulting in a steep drop-off in vaccination rates over the 50 months. Furthermore, given that the protection of Zostavax against shingles wanes rapidly each year following vaccination, there is a drastic reduction in protection levels compared to the amount of people vaccinated in Figure 2.2. Indeed, the highest level of protection in 2020 is again in the most vaccinated group, the 69 year olds, with only 36.93% of the entire subgroup being effectively protected, due to the efficacy of Zostavax starting at only 64% immediately following vaccination. We also see the protection in subgroups that were aged out of the eligibility window decrease quickly, as again, efficacy in the vaccine is impacted by time since vaccination. Numerical results for Figure 2.2 are also provided in Table A.2.

2.3.3 Ontario distribution of Shingrix: 2020 and beyond

To estimate future coverage in the 2020 updated shingles vaccination program, we keep the same values of parameters as in the previous section, including arrival rates, while accounting for changes in population sizes, price per treatment schedule, and overall vaccine efficacy. It is important to note that according to guidelines put out with the new Shingrix program, seniors who received Zostavax under the previous program cannot participate in the new program, even if they are still within the age cohort window [38]. As a result, we do not return Zostavax-vaccinated seniors to the subgroup pool, even if they are no longer protected against shingles. Population forecasts are provided in Table A.1, and are based on average Ontario growth rate trends for seniors over the last decade. Those who received Zostavax through iterations of the first program are removed from these population numbers when

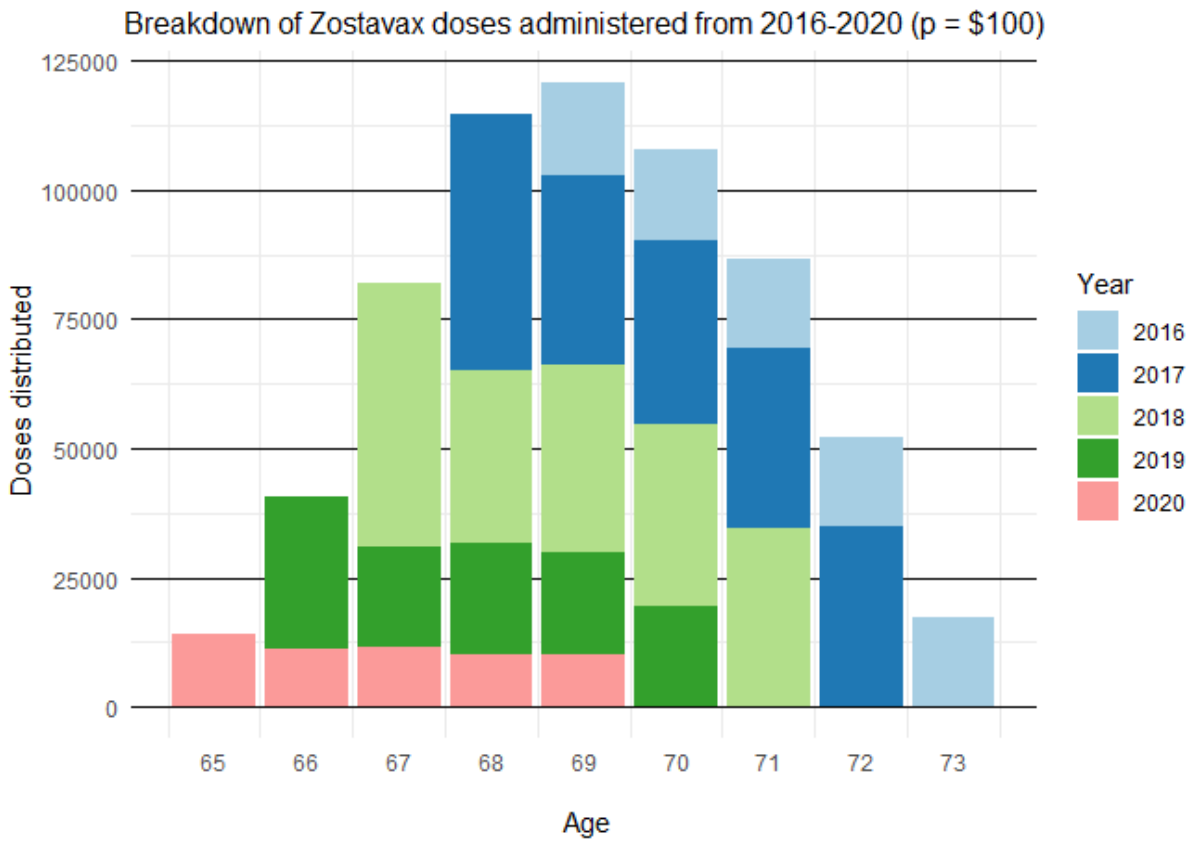

Figure 2.3: Total number of Zostavax doses allocated each year by age, 2016-2020 (price = $100). Vaccine allocation breakdown for all Ontarians who were age-eligible at some point for Ontario's publicly funded HZ immunization program between 2016-2020, assuming a 50% manufacturer's price discount. Note: exact group allocations may vary slightly between simulations each year due to the random order of group arrival in the DP distribution process, but yearly distributed totals remain the same.

applying the model to the Shingrix program. Additionally, Shingrix is a two-dose treatment, where as Zostavax requires only one shot. Shingrix is not approved to be administered as only one dose, so we assume that each unit of treatment for Shingrix represents a full vaccination course (two doses) in order to be able to make use of efficacy data.

For an estimate of Ontario's annual costs (the new program's budget), we look at the initial 3-year budget of the program in 2016 ($68 million) and understand it in the context of Canadian HZ healthcare costs per year ($67 million). Since Ontario's population was $\approx$ 38% of Canada's population in 2016 [39], Ontario would have had to spend roughly $\$67M \cdot 0.38 \approx \$25.5M$ a year in HZ healthcare costs, which, for 3 years, would have amounted to $\approx \$76M$. This means Ontario invested about 90% of expected HZ healthcare costs to fund the original program. Thus, for 2020, we estimate a yearly budget for the new program similarly. We inflate Canada's yearly HZ healthcare costs to $73 million in 2020 dollars, and calculate Ontario as having 39% of Canada's population by the start of the new program [39]. This means we can predict $\$73M \cdot 0.39 \approx \$28.5M$ in yearly Ontario HZ spending. Since the original budget was meant for 3 years, spending adds up to $\$85.5M$, and if we apply the same ratio of program spending to treatment spending in 2016, we estimate a budget of approximately $\$76M$ for the Shingrix program, independent of any other considerations. It is reasonable to expect HZ healthcare costs will continue to rise, as seniors are the fastest-growing age group in Ontario, not to mention the most at-risk for HZ. In fact, in 2016, seniors made up 16% of Ontario's population, and are expected to make up 25% by 2041 [2]. Many studies support that a higher investment in preventative measures now may offset future retroactive costs for HZ by a considerable and worthwhile amount [36, 40, 41, 42].

Shingrix costs approximately $300 for a full two-dose course, with 97.4% efficacy in 60-69 year olds, which we assume holds for 65-69 year olds [36]. We will also model to account for a 50% manufacturer's price reduction, and waning protection over time since vaccination using estimates from [23]. Model results for Shingrix are presented in Figures 2.4 and 2.5.

Table 2.5: Year-specific distributions of Shingrix at two price points.

	$p = \$300$	$p = \$150$
2020	45,500	45,500
2021	208,150	249,750
2022	0	207,250
2023	0	4,800
2024	0	0
Total	253,650	507,300

We find that the cost of a Shingrix program over 50 months when $p = \$300$ consumes the entire budget of \$76.095 million for 253,650 courses, again independent of operational costs, and that vaccines run out by November 2021 (roughly one year after the start of the new program). If that price is reduced to \$150, the budget is still exhausted, but acquires 507,300 courses. Assuming the lower course price, we estimate 45,500 courses distributed in the last two months of 2020, 249,750 in 2021, 207,250 in 2022, and 4,800 in 2023, with no courses left for 2024 (Table 2.5). Yearly distribution breakdown by age group over the whole program window is illustrated in Figure 2.6. The highest vaccinated age groups in 2024 are 69, 70, and 71 year olds, with nearly 70% of each subgroup receiving treatment over the course of the program, resulting in respective coverage rates around 62%. Exact results are given in Table A.2. Again, both demand and supply drop off in the later years of the program.

2.4 Discussion

2.4.1 Program impacts

Through the Zostavax program, assuming the 50% vaccine price discount, we estimate at having vaccinated 43% of all people who passed through the program age window between 2016 and 2020 (43% of people aged 65-74 in 2020). On average, our model distributed

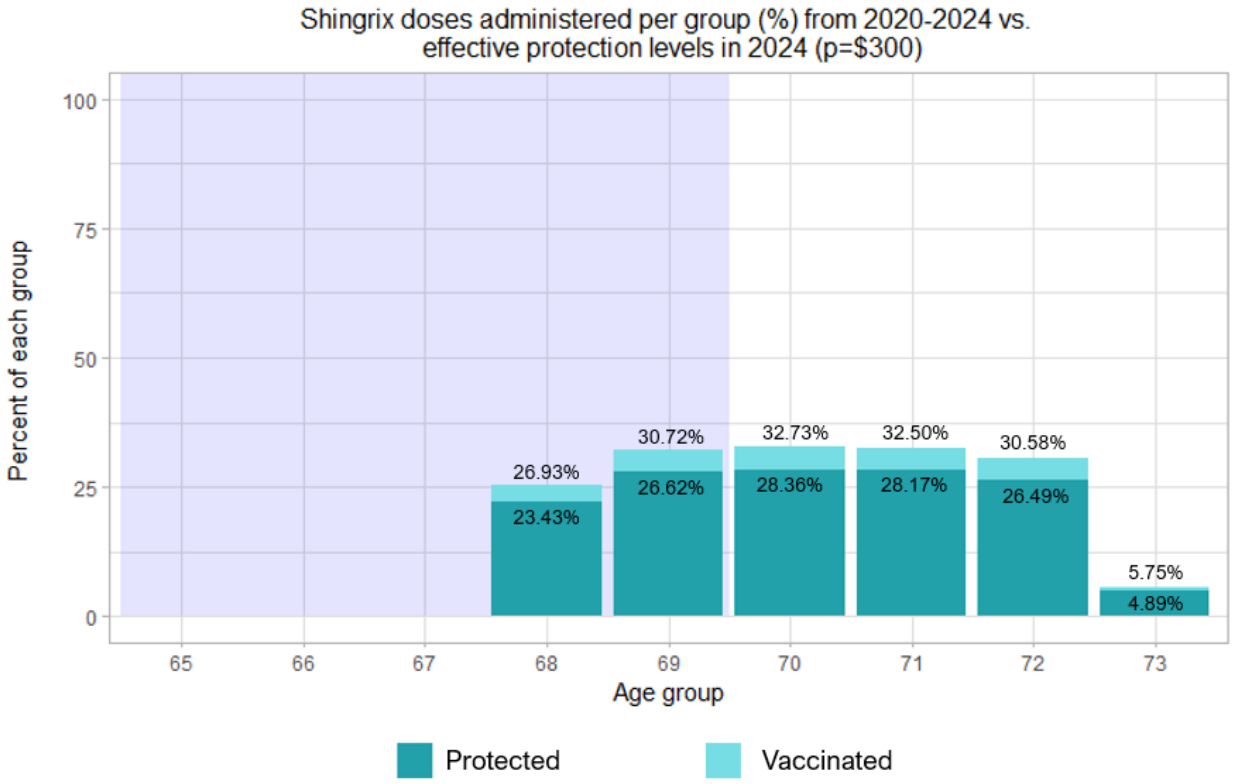

Figure 2.4: Percentage of individuals by age year who received Shingrix courses between 2020-2024, compared with resulting coverage levels in 2024 (price = $300). The five rightmost age groups represent those who were between 65-69 in 2020. The shaded region indicates the cohort of 65-69 year olds vaccinated in 2024.

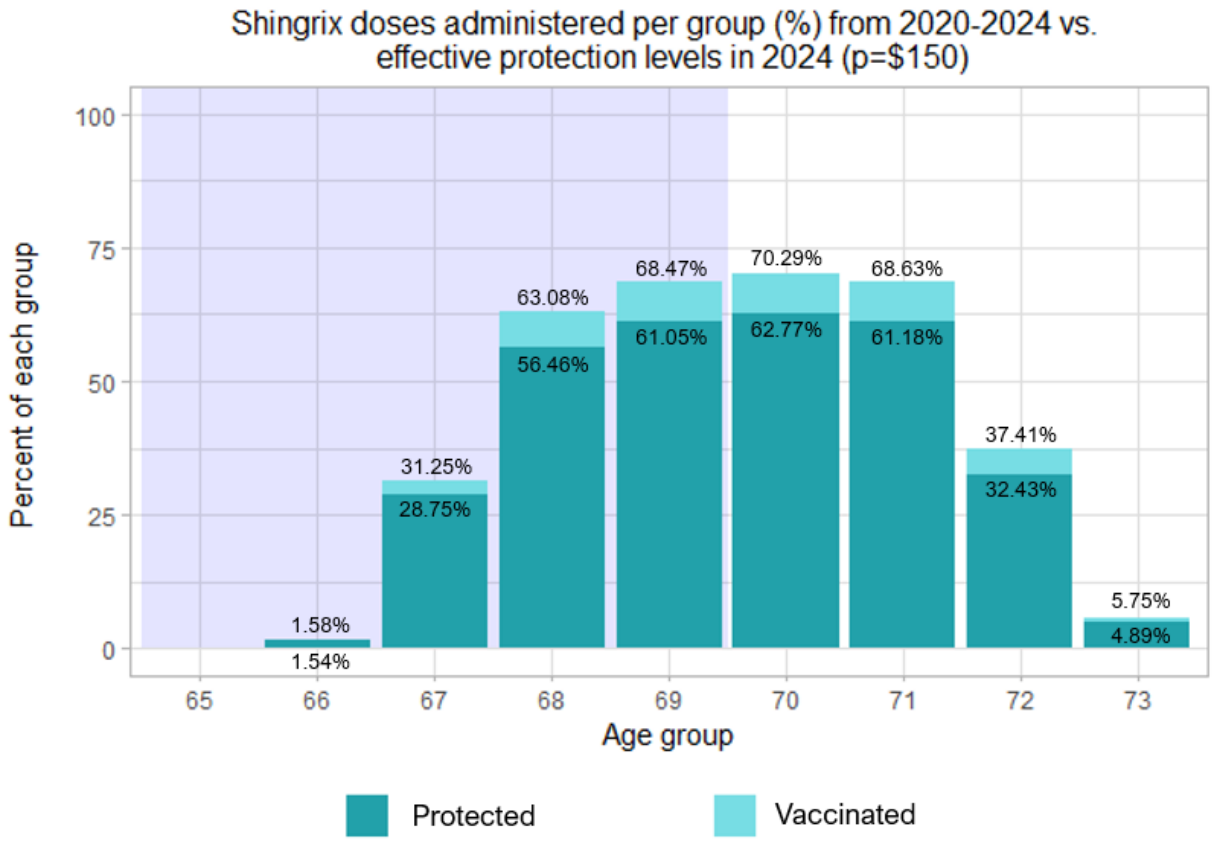

Figure 2.5: Percentage of individuals by age year who received Shingrix courses between 2020-2024, compared with resulting coverage levels in 2024 (price = $150). The five rightmost age groups represent those who were between 65-69 in 2020. The shaded region indicates the cohort of 65-69 year olds vaccinated in 2024.

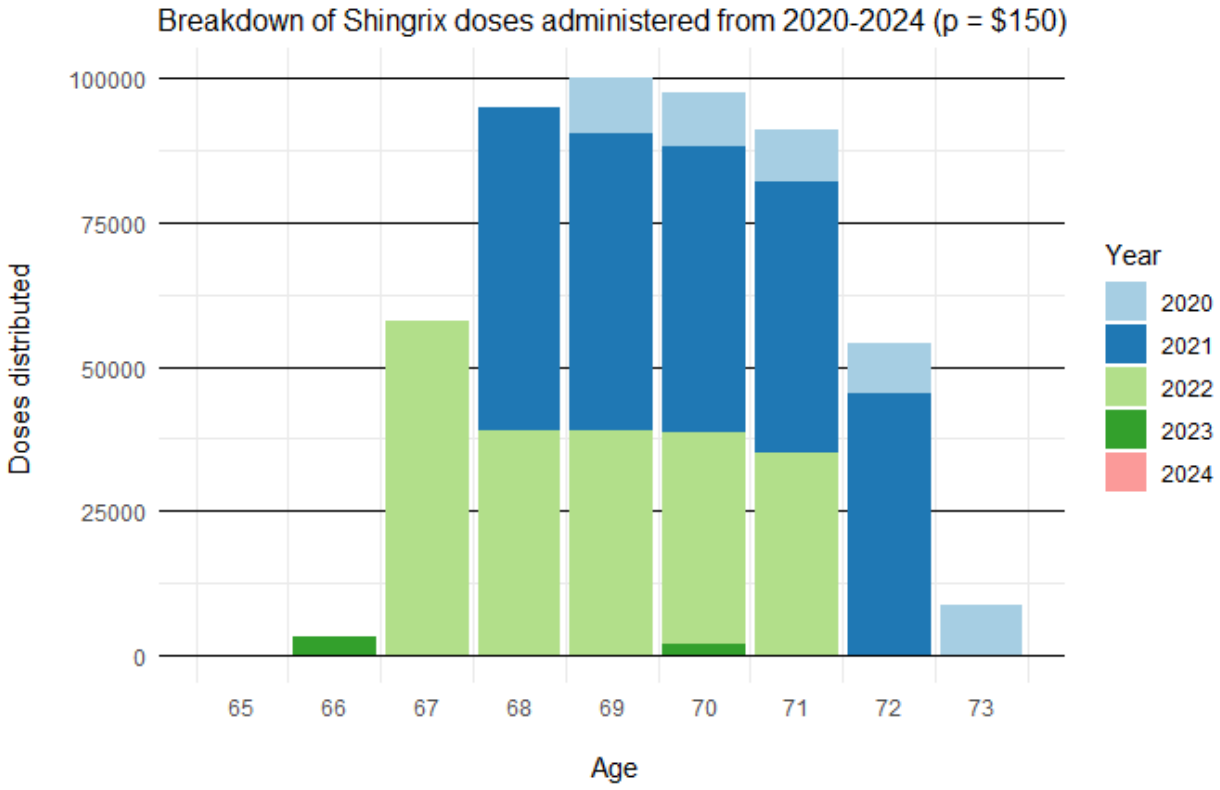

Figure 2.6: Total number of Shingrix courses allocated each year by age, 2020-2024 (price = $150). Vaccine allocation breakdown for all Ontarians who are age-eligible at some point for Ontario's publicly funded HZ immunization program between 2020-2024 (excluding those who had already received Zostavax), assuming a 50% manufacturer's price discount. Note: exact group allocations may vary slightly between simulations each year due to the random order of group arrival in the DP distribution process, but yearly distributed totals remain the same.

183,665 doses per year, or 19.95% of 65-69 year olds each year. More specifically, 12,720 doses were administered per month on average, or 1.66% of the eligible cohort per month for 50 months. Assuming 20.4% of Ontarians aged ≥ 50 had been vaccinated by 2016 with an additional 636,000 vaccinations by 2020 (assuming our lower pricing scheme), Ontario's HZ vaccination rate in people ≥ 50 will have grown to approximately

$$\frac{20.4\% \times (ON_{50+}(2016)) + 636,000}{ON_{50+}(2020)} = 30.5\%$$

by 2020 thanks to the Zostavax program alone. Of course, in reality, this is not to mention the potential impact of the COVID-19 pandemic on perceived importance and access to HZ vaccination in 2020, which may have significantly lowered demand that year compared to our projections.

With the Shingrix program and a 50% price discount, 37% of all people who pass through the program age window (and did not previously receive Zostavax) will become fully vaccinated between 2020 and 2024. Over the same 50 month time period, this equates to 18% of 65-69 year olds per year, or 1.5% per month. Despite the reduction in the number of initially eligible seniors starting in 2020 due to the previous program, higher incoming population sizes and prices constrain the ability of the Shingrix program to meet demand in the same amount of time. Clearly, for the Shingrix program to continue to be viable, more money will have to be invested to meet this level of demand for HZ vaccination and raise total population coverage. Costs aside, Figure 2.7 exemplifies the superior coverage provided by Shingrix across the population, particularly over time, offering a visualization of cost-effectiveness in favour of Shingrix's price tag.

Ontario's total HZ vaccination rate by 2024 will depend on both the pricing and demand in both programs, but will also be composed of individuals immunized with different vaccines with widely varying protection rates. By the end of 2024, any participant of the first program

Figure 2.7: Comparison of coverage (effective protection) conferred to those vaccinated with Zostavax between 2016-2020 versus Shingrix between 2020-2024. When compared over respective 50 month periods for each program, Shingrix clearly offers superior protection until the program runs out of doses.

will have less than 15% protection against shingles (see Figure 2.8). While the results of pilot program provide valuable insight for demand and total costs in the Shingrix program, based on the waning coverage demonstrated by our model for Zostavax, total national HZ vaccination rates may no longer serve as a valuable evaluation metric, given that the type of vaccine received will affect the true protection in a population.

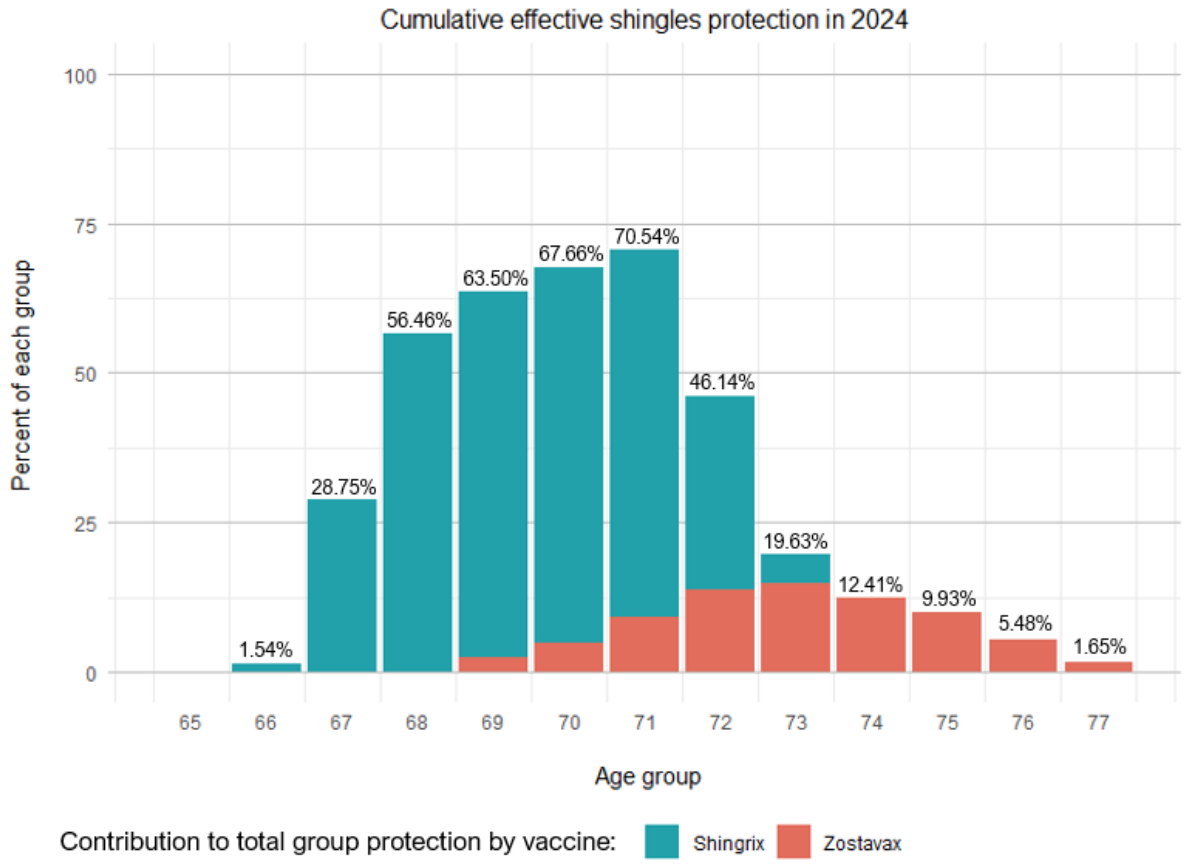

Figure 2.8: Population coverage (effective protection) in 2024 for recipients of Zostavax (price = \$100) from 2016-2020 versus Shingrix (price = \$150) from 2020-2024. Note that Zostavax's efficacy beyond 5 years since vaccination is not well documented, so the protection rate for anyone who received Zostavax earlier than 2020 is fixed at the Year 5 rate (14%) [35]. Thus, Zostavax's contribution to protection levels in 2024 are likely lower in reality than shown here.

2.4.2 Comparison to other HZ immunization programs

We examine HZ vaccination rates in three other countries for comparable coverage benchmarks to assess the performance of Ontario's program.

Zostavax has been available and recommended for seniors in the US since 2006. The National Health Interview Survey (NHIS) reports on HZ vaccine coverage among eligible adults, estimating that HZ vaccination rates in individuals ≥ 65 has increased from approximately 6.7% in 2008, to 31.1% in 2014, up to 39.5% in 2018 [43, 44, 45]. The NHIS also estimated that those ≥ 60 with health insurance were 1.5x more likely to receive an HZ vaccine than those without [43].

In England and Australia, HZ vaccination programs are funded for 70-79 year olds. The publicly funded program in England has offered Zostavax since 2013 and was evaluated in 2018 for both its routinely targeted age group (70 year olds) and its catch up cohort (71-79 year olds). Respective uptake rates were estimated from primary care and hospitalization records of vaccination at 62% and 57% respectively, and generally declined each year over the course of the program [19]. Australia began its program with Zostavax in November 2016, and data was collected from patient primary care records up until December 2018. Australia's national immunization register estimated 31.2% vaccination for its target age group within a year and a half of the program, but noted likelihood of underestimated figures since the doses distributed under the program far exceeded those reported to the registry [20]. Lin et al. (2020) used primary care records to extend these estimates, finding that average monthly vaccine uptake monotonically decreased from 5.5% in 2016 to 1.6% in 2018, with cumulative vaccination over this period reaching 46.9% [20].

Ontario's past and predicted uptake for shingles vaccines are certainly comparable to other established vaccination programs under the assumed model parameters. Additionally, our simulated arrival rates followed from those of other programs by implementing a progres-

sive decrease in demand from the initial start of the program. To improve vaccination rates, some jurisdictions establish vaccination targets. For example, the U.S. has a goal of 30% population HZ coverage for seniors ≥ 60 [46]. Canada has no such national target for HZ, but does for other diseases like influenza, which has a much higher coverage rate [23]. This could imply that efforts by physicians to advertise shingles vaccination in order to meet such targets may play a role in higher uptake levels, which may offset Shingrix's higher course price by saving future HZ-related medical costs in Ontario. The new program in Ontario may also consider following the lead of England and Australia, offering a supplementary catch-up cohort to those aged 70-74 over the next 5 years (those who were 65-69 in 2016) to vaccinate or revaccinate those who passed through the first program's window and bringing true protection rates closer to the reported HZ vaccination level.

2.4.3 Assumptions

The accuracy of our model's results depends on several assumptions. First, we assume that demand forecasting is accurate, having been determined via uniform arrival rates calculated from NACI coverage estimates and Canadian population data, and lowered over time in a comparable fashion to rates reported in England and Australia. Second, we do not account for shortages or surpluses in vaccines available per unit time, assuming supply meets demand perfectly until the budget runs out. Third, vaccine efficacy rates are reported in 10-year intervals after age 50, and so the 60-69 year old rates are assumed to apply for 65-69 year olds. Another large assumption in the modeling of Shingrix is that every unit of treatment administered in our model represents a full two-dose vaccination schedule, which implies that everyone who receives their first shot also receives their second. Cost-effectiveness and protection rates may differ if uptake of the second dose is wildly lower than the first dose. While more people may be able to get vaccinated if doses are not reserved to finish full

vaccination courses, a single dose of Shingrix is not approved as a treatment and there have been no clinical studies to assess the protection from only one dose, so we do not explore this as a scenario, but it may be of interest in future work [47, 48, 49]. Furthermore, we assume no major changes in population growth by 2024, nor do we account for individuals purchasing and vaccinating with Shingrix privately in population or coverage estimates. Another assumption affecting the total number of vaccines available is the government price discount, which may vary from what we have simulated here (50%). Finally, we assume that in general, the development of the COVID-19 pandemic does not influence the demand or availability of shingles vaccination in the new program.

2.5 Conclusion and future work

Through this model, we have provided a method of estimating yearly and monthly maximal vaccine coverage for an immunization program, which can be used to help tailor spending estimates for the current HZ program and potential programs in other regions. Through its pilot program, we predict Ontario will have potentially increased its HZ vaccination rate in people aged 50 or older from 20.4% in 2016 to 30.5% in 2020 by publicly funding vaccination for 65-69 year olds, who make up an increasing proportion of total seniors each year. However, since the protection from Zostavax for individuals in the first program falls below 15% after 5 years, this vaccination level is not reflective of the true level of protection in the population. We also demonstrate the superior protection levels conferred by Shingrix in this age group, which may encourage other countries to consider updating the standard of care in their HZ programs.

It should be noted that the uptake and total coverage projections produced here for Shingrix are highly dependent upon assumptions made for the delivery of the Zostavax program, as well as assuming perfect adherence to Shingrix's two-dose schedule. In future

work, our predicted results for the Zostavax program should be compared with the upcoming 2021 aNICS coverage survey results for HZ, which will offer a new benchmark of Canadian shingles vaccination uptake to date and allow for fine-tuning of parameters used in the model. Including variable completion rates of a full course of Shingrix will also result in wider ranges for coverage estimates, providing lower and upper bounds for costs and program effectiveness.

Additionally, our model could be used to explore future adjustments to the program's design. For example, age windows could be widened to simulate an expanded vaccination schedule, incorporating Shingrix's longer protection estimates. Other countries already publicly fund 70-79 year olds, and data suggests that younger age groups tend to show higher uptake levels. Extensions could also be made to reformat this model so as to make it applicable for the optimal distribution of vaccines for infectious diseases, where the timeline of distribution becomes much more important for preventing outbreaks.

Finally, there are other ways to approach the problem tackled here. One might consider incorporating uncertainty in estimated demand to reflect non-uniform arrival rate distributions. Furthermore, the method of dynamic programming may be supplemented with alternate optimization solvers, such as CPLEX or MATLAB's optimization toolbox for more generalized solutions.

Chapter 3

Age-stratified transmission model of COVID-19 in Ontario, Canada with human mobility during pandemic's first wave

R. Fields, L. Humphrey, D. Flynn-Primrose, Z. Mohammadi, E. W. Thommes, and M. G. Cojocaru. Age-stratified transmission model of COVID-19 in Ontario with human mobility during pandemic's first wave. *Submitted to: Heliyon Mathematics,* 2020.

Abstract

In this work, we employ a data-fitted compartmental model to visualize the progression and behavioural response to COVID-19 that match provincial case data in Ontario, Canada from February to June of 2020. This is a "rear-view mirror" glance at how this region has responded to the 1st wave of the pandemic, when testing was sparse and NPI measures were

the only remedy to stave off the pandemic. We use an SEIR-type model with age-stratified subpopulations and their corresponding contact rates and asymptomatic rates in order to incorporate heterogeneity in our population and to calibrate the time-dependent reduction of Ontario-specific contact rates to reflect intervention measures in the province throughout lockdown and various stages of social-distancing measures. Cellphone mobility data taken from Google, combining several mobility categories, allows us to investigate the effects of mobility reduction and other NPI measures on the evolution of the pandemic. Of interest here is our quantification of the effectiveness of Ontario's response to COVID-19 before and after provincial measures and our conclusion that the sharp decrease in mobility has had a pronounced effect in the first few weeks of the lockdown, while its effect is harder to infer once other NPI measures took hold.

3.1 Introduction

Since December 2019, the novel betacoronavirus SARS-CoV-2 and its associated disease COVID-19 have spread from the point of origin in Wuhan, China [50] to virtually all corners of the globe. As of May 1, 2021 over 150 million people worldwide have been confirmed as having contracted COVID-19, resulting in over 3 million deaths. Despite the recent development and ongoing distribution of several vaccines, the total number of cases is increasing [51]. Predictably, the events of the last year have stimulated a robust discussion related to the nature of mathematical models in epidemiology as they inform public policy [52, 53, 54]. It seems prudent then, before describing our own model and results, to review the history of mathematical modeling in epidemiology and to recall the challenges it continues to pose.

3.1.1 Background

The mathematical theory required to effectively model the spread of infectious diseases throughout a homogeneous population was developed by Gottfried Leibniz in the latter half of the 17^{th} century [55, 56, 57]. Leibniz's work was quickly put to use describing physical systems by early physicists, notably Jacob Bernoulli in 1695 [58]. Early contributions to the mathematical study of infectious diseases began appearing during the 18th century notably by the physicist Daniel Bernoulli in 1760 [59]. In 1866, during an epidemic of cholera in London, William Farr appears to have been the first person to (publicly) employ mathematics to predict the likely course of an epidemic [60, 61, 62]. His projection was apparently based on simple curve fitting and was seen as successful by his contemporaries, but attempts to extend his ideas to a more general context proved disappointing [62]. Further, more successful efforts to derive a mathematical model of epidemics were undergone by Brownlee [63, 64], Ross [65] and Hudson [66, 67]. The so-called 'SIR' model common in modern epidemiology was arrived at in 1927 by Kernack and McKendrick [68]. In the simplest case this type of model divides the population into three compartments: "susceptible", "infected", and "recovered". Differential equations can then be used to describe the movement of the population between the compartments. Unfortunately, this simple model has two disadvantages which render it unsuitable for most practical purposes. Firstly, for an SIR model to produce accurate results it must use accurate values for its parameters (e.g. rate of transmission, recovery time, and mortality rate). These parameters can be difficult to measure and may not be constant across an entire population. The second disadvantage of SIR-type models is that they assume that the population in any given compartment is homogeneous, which can cause them to ignore important differences such as age, location, and travel habits. Mathematically this can always be resolved by adding more compartments, however this increases both the computational complexity of the model and the number of parameters needed to produce

an output. For these reasons, contemporary models, while still recognizably related to the classic SIR model, are typically modified to accommodate the specifics of the pathogen being modeled, important variances in the population, and the intended purpose of the model [69, 70, 71, 72, 73, 74].

Some early models for the COVID-19 outbreak returned to curve-fitting as a method for projecting future outcomes [75]. Much of the epidemiological modelling is now performed with variants of the classic SIR model [76, 77, 78, 79] which fits the number of individuals in a population who are susceptible to, infected with, or have recovered from a communicable disease. The model can be extended to incorporate different phases of a disease [80], or population subtypes [81]. Studies have stratified Ontario populations by categorising gender [82] or profession (such as healthcare workers) [83] separately. Age has also been shown to play an important factor in the transmission of COVID-19 [84] and in this paper we will further investigate that variable.

Although contact rates between individuals have previously been studied [85, 86], due to imposed social distancing and sheltering measures, absolute contact rates during the pandemic have changed drastically from baseline. Presently, governments have imposed measures in an attempt to reduce the spread of COVID-19. These include sheltering in place and quarantining, travel restrictions, social distancing protocols, and the closure of public and commercial spaces. Specifically in Ontario, the government has mandated a slow relaxation of shelter-in-place measures and reopening of the economy throughout the late spring and summer of 2020 [87], and provided guidance on protective measures such as hand-washing and the use of face coverings.

Naturally, there is considerable interest in understanding the effects of the measures taken to mitigate the spread of COVID-19 [88, 89, 90], and at this stage, a year into the pandemic, looking back to what can be learned is as important as forecasting the next pandemic wave. A comparative study used Google mobility data for Canada, not to model the epidemic,

but to assess governmental interventions and social distancing measures, and to compare Canada's response with that of other countries [91]. A Texas study assumed two situations using arbitrary values: a 90% drop in contacts for individuals in self-isolation and a 40% drop in contacts for those practising social distancing [92]. More accurate estimates may be gained through anonymised location data gathered from mobile phones. Using a combination of proprietary and publicly available data, it has been shown in the United States that the adoption of shelter-in-place policies corresponds to a sharp decrease in mobility. It has also been shown that the number of identified cases is directly correlated to mobility [93, 94] in February-April 2020, which is something we see here as well. However we also show that increased mobility in the population of Ontario stops being a good indicator of pandemic evolution past April 2020. This is likely due to the fact that while mobility has steadily risen, other NPI measures took hold, such as mask wearing, and larger testing capacity.

To estimate differences in contact during the epidemic, a team of researchers using an SEIR-type model found the overall contact-rate in British Columbia dropped by 78% due to distancing and isolation measures. The paper, however, only uses mobility data to determine the beginning and end dates of these measures, without considering that mobility will change over time due to relaxed restrictions [95]. Related studies done for France [96] and the UK [97] found similar values, in that overall contacts were reduced by 70-80 %.

It is known that the contact rates between individuals of different age groups will vary significantly [98], so it is important to take this into account. An Ontario paper uses an SEIR-type model with compartments by age, but only modifies the severity of infection per age group [81]. A Brazilian study uses data from nine distinct age groups, but uses identical contact rates within and between groups [99]. [100] uses an SEIR model with age stratification to investigate the effect of various management strategies. Unfortunately, the study suffers from a lack of empirical data instead arriving at exposure rates by "making educated estimates of the effects of hygiene restrictions and specific social interactions in

each place". The spread of the disease is greatest between adults in the same age group, and less frequently between parents and children. These results will have an impact on the effective contact rates between individuals [101].

In our work, we use age-stratification in three broad age groups: young (less than 20 years), adults (between 20 and 60 years) and seniors (60 years and older). We use Ontario's public health onset case data [102], we use the Google mobility data for Canada, and we adapt the contact rates, per broad age groups from existing literature. We adapt an SEIR-type model and we successfully fit the onset case data in Ontario, per each age category, to the simulated symptomatic cases, while discounting outbreak cases in long-term care (as median age there is higher than our modelled population groups). The period of time of interest for us is February - June 2020.

In our work, we quantify the level of pandemic mitigation in Ontario via the study of a behavioural coefficient q, which represents the decrease in base contacts due to lockdown and social-distancing measures. Moreover, we show that this reduction coefficient can be looked at as having two important contributors: the first is from mobility reduction in the province (at work, outdoor, retail, schools, etc. categories), while the second is due to all other NPI measures that have started to take hold or be required, such as mask wearing, restricted commerce and services, etc. We can clearly see then that mobility reduction has certainly had a pronounced impact on contact reduction in the first 4 weeks after the first lockdown was imposed, however it becomes a poor indicator (if at all) of pandemic evolution beyond that short time frame.

The structure of the paper is as follows: in Section 2 we present our methods and materials, in Section 3 we present our calibration results and reduction factor discussion, and then we close with some concluding remarks and future work.

3.2 Methods

3.2.1 Adapted SEIR model

We introduce an adapted SEIR model to the question at hand by modifying and age-stratifying a variant of the SEILR model presented in [103] and [104]. First, we refine the Infected compartment further into three compartments: presymptomatic (I^P), asymptomatic (I^A), and symptomatic (I^S). In this way, we may better examine the dynamics of the COVID-19 infection through its stages of development and consequent patient behaviour due to symptom prevalence.

Second, we generalize the model to allow for age group stratification and interactions between groups. In short, we propose the **extended SEILR(pas) model** with the following compartments: Susceptible (S), Exposed (E) - not yet contagious, Infected (p)resymptomatic (I^P) - contagious, Infected (a)symptomatic (I^A), Infected (s)ymptomatic (I^S), Recovered (R), and iso(L)ated - symptomatic cases isolated to prevent spread.

In order to account for differences in disease susceptibility and infection outcomes, we divide the population of Ontario (the most populous province of Canada) in three age-stratified subgroups: Group 1, denoted by N_1: 0-19 years old, Group 2, denoted by N_2: 20-59 years old, and finally Group 3, denoted by N_3: ($\geq$ 60) years old.

Contact rates (c_{ij}) within and between these age groups groups were inferred from Canadian contact data estimated by Prem, Cook, & Jit (2017) [86], who projected social contact patterns in 152 countries (see sec:appendix3 for details). Since contact rates are a factor in determining the size of the effective contact rates, typically denoted by β, in the context of age-stratified transmission, the effective rates will be denoted by β_{ij}. Before we outline the equations governing our model, we include first the flow chart between the above compartments, together with classic notations of the flow rates in Figure 3.1.

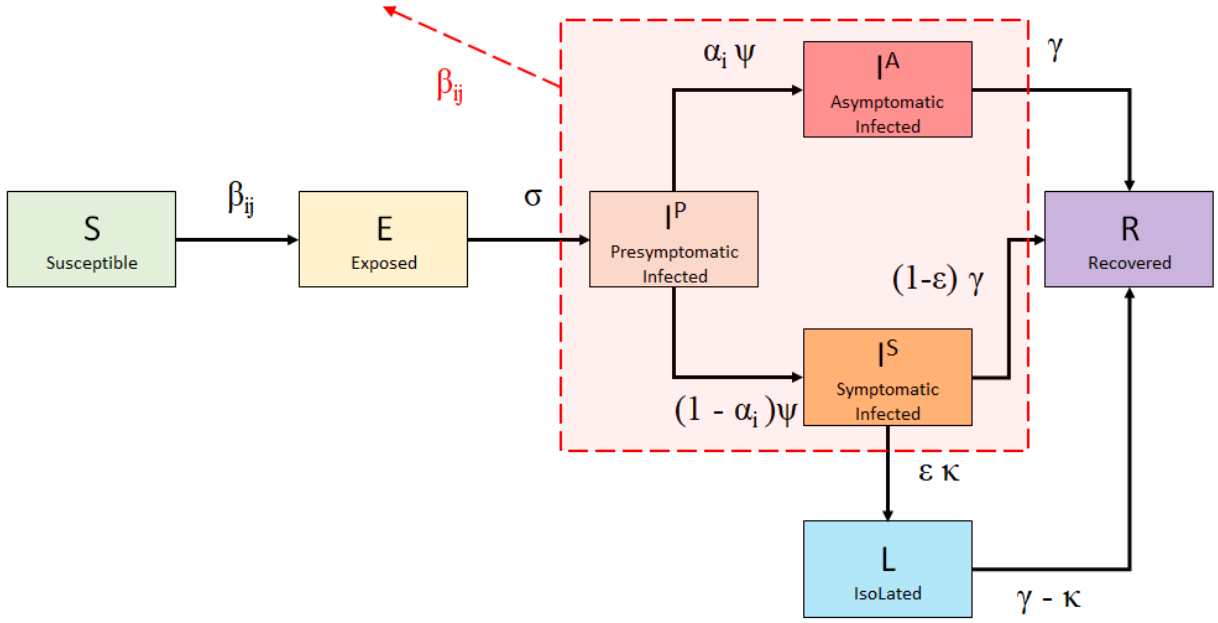

Figure 3.1: Schematic of SEILR(pas) model for COVID-19 progression and control measures for a Group i, $i \in \{1, 2, 3\}$. The outward arrow labelled β_{ij} implies that the encircled compartments (Presymptomatic, Asymptomatic, and Symptomatic infected) in each age group have an impact on new transmissions to the other age groups $\{1, \ldots, 3\}$.

Considering the i-group model for $i, j \in \{1, \ldots, K\}$, the differential equations governing each of the groups are given by:

$$\begin{cases} \dfrac{dS_i}{dt} = -\displaystyle\sum_{j=1}^{K} \beta_{ij} S_i(t) \frac{I_j^P(t) + I_j^A(t) + I_j^S(t)}{N_j(t)}, \\ \dfrac{dE_i}{dt} = \displaystyle\sum_{j=1}^{K} \beta_{ij} S_i(t) \frac{I_j^P(t) + I_j^A(t) + I_j^S(t)}{N_j(t)} - \sigma E_i(t), \\ \dfrac{dI_i^P}{dt} = \sigma E_i(t) - \psi I_i^P(t), \\ \dfrac{dI_i^A}{dt} = \alpha_i \cdot \psi \cdot I_i^P(t) - \gamma I_i^A(t), \\ \dfrac{dI_i^S}{dt} = (1 - \alpha_i) \cdot \psi \cdot I_i^P(t) - (1 - \epsilon)\gamma I_i^S(t) - \epsilon \cdot \kappa \cdot I_i^S(t), \\ \dfrac{dR_i}{dt} = \gamma(I_i^A(t) + (1 - \epsilon) I_i^S(t)) + (\gamma - \kappa) L_i(t). \\ \dfrac{dL_i}{dt} = \epsilon \cdot \kappa \cdot I_i^S(t) - (\gamma - \kappa) L_i(t). \end{cases}$$

Individuals are all initialized in the S compartment, with the exception of a single infected individual from the largest group seeded in the I^P compartment. Susceptible individuals exposed to the virus enter the E category for an average of $1/\sigma$ days before they become contagious, at which point they move into the I^P category. After an average of $1/\psi$ days, $1 - \alpha$ proportion of individuals will develop symptoms and move into the I^S compartment, with the remaining α moving into the I^A compartment. Individuals in I^P, I^A and I^S compartments are all contagious. ϵ proportion of individuals in I^S choose to self-isolate to prevent further disease transmission, and as a result move into compartment L (isolated) and do not interact with others. They do so with a delay of $1/\kappa$, accounting for test result waiting time and individuals who may disregard minor symptoms initially. $1/\gamma$ days after

entering the I^A and I^S compartment, individuals all recover from (or succumb to) their infection and move into the R compartment, where they remain permanently. The model was implemented and numerically solved with R (version 4.0.2) using the package *deSolve*.

3.2.2 Ontario specific parameter values and data sources

We assume that the outbreak of COVID-19 in Ontario begins on February 14, 2020, and that the implementation of intervention and control strategies begins on March 15, 2020. Control responses in Ontario were officially enacted on Monday, March 17, [105], but commensurate with earlier institutional responses, we adjust for the fact that the public began to alter behaviour before this date. For further discussion, see the sec:appendix2 section in the Appendix. We assume individuals who recover from infection remain in the R compartment, with immunity from COVID-19 for the duration of the simulation. Given the short time frame for simulation, our model does not include births or natural deaths, and any COVID-19 deaths are captured in R. Furthermore, we assume an isolation delay of one day on average, due to individuals not always taking initial symptoms seriously enough to isolate.

Additionally, we assume an isolation compliance rate of 95%. An early study of the virus in quarantined cruise ship passengers finds that 17.9 % of infected individuals were asymptomatic, and suggests the true proportion could be up to 39.9 % depending on the latency period of the virus [106]. A meta-analysis of six studies estimates the asymptomatic infection rate to be anywhere in the range of 18.4 % to 78.3 %, and cites 46 % as the most likely value [107]. We use the age stratified symptomatic rates found by Davies et al. (2020) [84] for our model, as shown in Table 3.1. Next, we assume that the only cases reported by Ontario's public health units (PHUs) are symptomatic cases, and that every symptomatic case will be identified and reported. In addition, we assume that asymptomatic and presymptomatic cases are not tested and therefore do not self-isolate.

The model presented above is now tailored to Ontario using the parameter values in Table 3.1, as well as Ontario data sources for the pandemic evolution to date.

Symbol	Definition	Initial Value	Reference
K	Number of age groups	3	
N_i	Subgroup population size		
	N_{total}	14 566 547	[108]
	N_1: (0-19)	3 141 693	[108]
	N_2: (20-59)	7 977 131	[108]
	N_3: (60+)	3 447 723	[108]
c_{ij}	Number of daily contacts with Group j per member of Group i	Table 3.2	
p	Transmission probability per contagious contact	Section 3.2.5	
β_{ij}	Effective contact-rate, $i, j \in \{1, \ldots, K\}$	$c_{ij} * p$	
σ	Time from exposure until contagious (days)	1/2.5	[81]
ψ	Time from contagious until symptomatic (days)	1/3.5[1]	[81],[109]
α_1	Proportion of permanently asymptomatic cases in N_1	0.963	[84]
α_2	Proportion of permanently asymptomatic cases in N_2	0.7	[84]
α_3	Proportion of permanently asymptomatic cases in N_3	0.35	[84]
ϵ	Proportion of compliance with isolation	0.95	assumption
κ	Isolation delay	1	assumption
γ	Recovery/removal rate	1/7	[80]

Table 3.1: Parameters and initial values of the SEILR system (3.2.1).

3.2.3 Deriving contact rates for Ontario pre-pandemic

We first need to derive contact rates within and between the three stratified age groups introduced above. There are many examples in infectious disease modelling literature that assume uniform contact mixing for simplicity (for example, modelling Ebola dynamics in [110]), however, such an assumption neglects the significant role that age may play in relevant

[1]The parameter ψ is estimated from the relationship $1/\sigma + 1/\psi$ = incubation period, where $1/\sigma = 2.5$ days and incubation period = 6 days.

contact patterns [111]. The Ontario groups were partitioned as such to characterize different contact rates associated with each age group.

Group 1 represents individuals in the youngest age group (0-19). As these individuals are school-aged, they generally experience high levels of interaction with similar-aged peers, as well as some interactions with individuals in Group 2, likely including their parents and other child care providers. Group 2 represents the majority of the working population (20-59). These individuals display very high levels of interactions with other adults, likely as a combination of workplace interactions, errands such as shopping, appointments, and peer-relationships, and moderate levels of interaction with Group 1 members. The majority of these interactions are likely with their own children, but this value may be skewed up in part due to child care supervisors in Group 2 having many interactions per day. Group 3 is the oldest age group and considers seniors and retirees (60+), who make comparatively fewer overall contacts than their younger counterparts. This is to be expected as many of these individuals are retired and thus their lifestyles are more likely to be leisure-oriented ([112], [113]). Based on low transmission probability due to low contact rates, Group 3 has the lowest chance of contracting COVID-19, although they carry a much higher risk of hospitalization if they do so [114].

From [86] (a study of country-specific contact rates), a 16x16 contact matrix of contact rates between Canadians aged $0-80$ was collapsed to create a condensed 3x3 contact matrix stratified by our selected age groups. See B.1 for details.

From Table 3.2, a high degree of assortativity (intra-group contact) was found in Groups 1 and 2, shown in boldface. Group 1, comprising children and students, are most likely to interact with their peers (63% of contacts), followed by adults (parents, teachers, etc. forming 34% of contacts), with very little contact with seniors (2% of contacts). Group 2 has the highest overall number of contacts, with adults coming into contact with other adults an estimated 77% of the time. Both results may be explained by Group 2 making up the

majority of the working age population, as well as holding positions requiring interaction with elderly or very young individuals (e.g. care workers, teachers). Interestingly, Group 3 individuals, while having the lowest number of overall contacts, have the most balanced spread of contact rates, and even perform contacts with Group 2 more than their own age group (53% vs. 29%, respectively). This may be due to interactions with health care workers and employees at various businesses (cashiers, wait staff, etc.), and the fact that some individuals may still be part of the workforce. We preserve our contact structure by adopting Canadian relative contact rates from [86] and assume they apply to Ontario for our time period with uniform contact scaling across all interactions. We assume our age-stratified population subgroups are homogeneously mixed, with hetereogeneous intergroup mixing.[2]

3.2.4 Case onset and mobility data

Tracked data for COVID-19 cases in Ontario were taken from Ontario's https://data.ontario.ca/en/dataset/positive-cases-of-covid-19-in-ontariointegrated Public Health Information System (iPHIS). This data set is compiled from reports from Ontario's PHUs, recording all confirmed cases of COVID-19 and qualitative factors for each case, including age group (by decade), gender, testing location, and patient outcome. In addition, iPHIS is one of the few data sources that provides both episode (case onset) date, as well as reporting date. Most other sources, including the https://www.cdc.gov/coronavirus/2019-ncov/cases-updates/cases-in-us.htmlCDC, only sort cases by reporting date. Cases organized by reporting date are highly subject to delays, including testing and submission delays, lab delays, and individual decisions regarding how soon after symptom onset one chooses to get tested. This produces noisier trend lines and both over- and under-estimates for daily counts. Since case-onset

[2]Since [86] estimates contact rates only up to 80 years of age, we assume that Ontarians aged 80+ have identical contact rates to those aged 60-80 years.

data is much more accurate, we chose it to match our simulated infection curve(s) in order to provide a more complete understanding of how transmission has changed over time since the pandemic onset.

We also incorporate some movement and behavioural activity in the population by considering Ontario mobility data compiled from Google's https://www.gstatic.com/covid19/mobility/2020-07-21$_C A_M obility_R eport_e n.pdf COVID-19 Community Mobility Reports. Specifically, we try to capture cha lockdown) activity in six broad categories : retail/recreation, groceries/pharmacies, parks, transit stations

To determine the pre-lockdown average contact rate for Ontario, we used the contact rates provided by Prem et al. [86] for Canada. We weighted the average contact rates of Canada with the Ontario population to get a daily average contact rate for an individual in Ontario. We considered this value as the average baseline (pre-lockdown) contact rate, i.e.:

$$contact_{av} \approx= 12.5046$$

To find the mobility-influenced time-dependent contact rates post-lockdown, we considered the average contacts rate in Ontario for the home, work, and other location categories (comprising retail/recreation and groceries/pharmacies) from Prem et al., ($\approx$ 3.2, 4.5, 3.8, respectively). Next, we used these category rates to modify the same categories of mobility data as follows:

$$contact^m_{av}(t) = contact^m_{av} \cdot g^m(t) \text{ where } m \in \{\text{Home, Work, Other location}\}$$

where the t unit is time=1 day and where $g^m(t)$ is the percentage increase or decrease in the category m of mobility as compared to Google's baseline values per category. Finally, we amalgamated the Google mobility-influenced contact rates of these categories to compute the daily mobility-influenced contact rate, by considering an average number of daily hours

an average Ontarian spends in each category, i.e., 8 hours of day for work, etc.

We thus assume that changes in Google mobility data as compared to baseline activity reflect equivalent changes in contact rates as compared to average contact baseline. We also assume that the proportion of the population that has opted to provide location tracking data to Google via their personal account settings can be considered representative of the behaviour of the total population of Ontario at large.

3.2.5 Dampening contact rates to replicate behavioural changes and preventative measures

The effective contact rate for a member of Group i with members of Group j is given by

$$\beta_{ij} = c_{ij} \cdot p, \tag{3.1}$$

In Davies et al. (2020), authors estimated p for COVID-19 in several models under different parameters, including susceptibility/asymptomatic rates and demographic structures. They found p values of 0.046 and 0.055 in Wuhan, 0.074 in Beijing, 0.084 in Lombardy, and 0.099 in South Korea [84]. For Ontario-specific studies, Abdollahi et al. (2020) found p ranging from 0.018-0.041 [115], and Wu et al. (2020) found p of 0.145 [116]. For our model, we solve for p implicitly, fitting to the onset data recorded by iPHIS for our pre-intervention period (Feb 14 - Mar 15). We do so using a derivative-free optimization method known as the Golden Section Search algorithm to minimize the sum of squared errors (SSE) between our model output and iPHIS data (see [117]).

We find that for the pre-lockdown phase, the corresponding transmission rate in Ontario is $p = 0.045$. We note that this transmission rate is much lower than the estimate of 0.145 given by [116], yet on par with the estimates given by [115]. We attribute the large difference

in transmission rate compared to [116] to two main factors. Firstly, their infectious period is 5 and 7.2 days for symptomatic and asymptomatic individuals respectively. In comparison, we use an infectious period of 10.5 days in our model, allowing for many more days of contacts while infectious. Secondly, their contact rates are lower than we consider here, with a universal contact rate of < 11.8, as opposed to our contact matrix which averaged ≈ 13 contacts per individual per day. As a result of fewer daily contacts in conjunction with fewer infectious days, one drastically reduces the total contacts each infected individual makes before recovery. To compensate for fewer contacts, a much higher transmission probability is required to produce similar case numbers.

Figure 3.2 depicts our simulated data from February 14 - March 15. After March 15, 2020, both the social behaviour and the mobility of the population have changed, as the province adopted various preventive measures to help curb the spread of COVID-19. (For more detail on date selection, see sec:appendix2 in the Appendix.) We therefore need our model to reflect changes in the frequency of contacts due to social distancing measures intra- and inter-groups, and changes in the transmission probability due to mask wearing and other hygiene practices.

To do so, we introduce a dampening variable, denoted by $q_{int} \in [0, 1]$ during a given time interval and generically denoted by int, such that

$$\beta_{ij}(int) = c_{ij} \cdot p \cdot q_{int}, \quad \forall\ int \in interval \tag{3.2}$$

where q_{int} is constant during time interval int, $interval$ is the number of time intervals used in the model, and int is defined as the ceiling of the number of weeks since preventive measures are introduced. Since no preventive measures were present pre-lockdown (February 14 - March 15), we will define this time period as int 0 := [Feb 14, March 15] and $q_0 := 1$. We use the Golden Section Search to fit our model to iPHIS data, but this time we fix

	Group 1	Group 2	Group 3	Total Contacts
Group 1	c_{11}=**8.565645854**	c_{12}=4.661272358	c_{13}=0.304014985	13.5309332
Group 2	c_{21}=2.987996842	c_{22} = **11.49063721**	c_{23} = 0.522285468	15.00091952
Group 3	c_{31} = 1.248771202	c_{32} = 3.686037351	c_{33} = 1.982952539	6.917761092

Table 3.2: Contact rates calculated for the three Ontario population subgroups. Contact rates are taken from Canadian estimates by [86] and weighted according to census data from Statistics Canada [108].

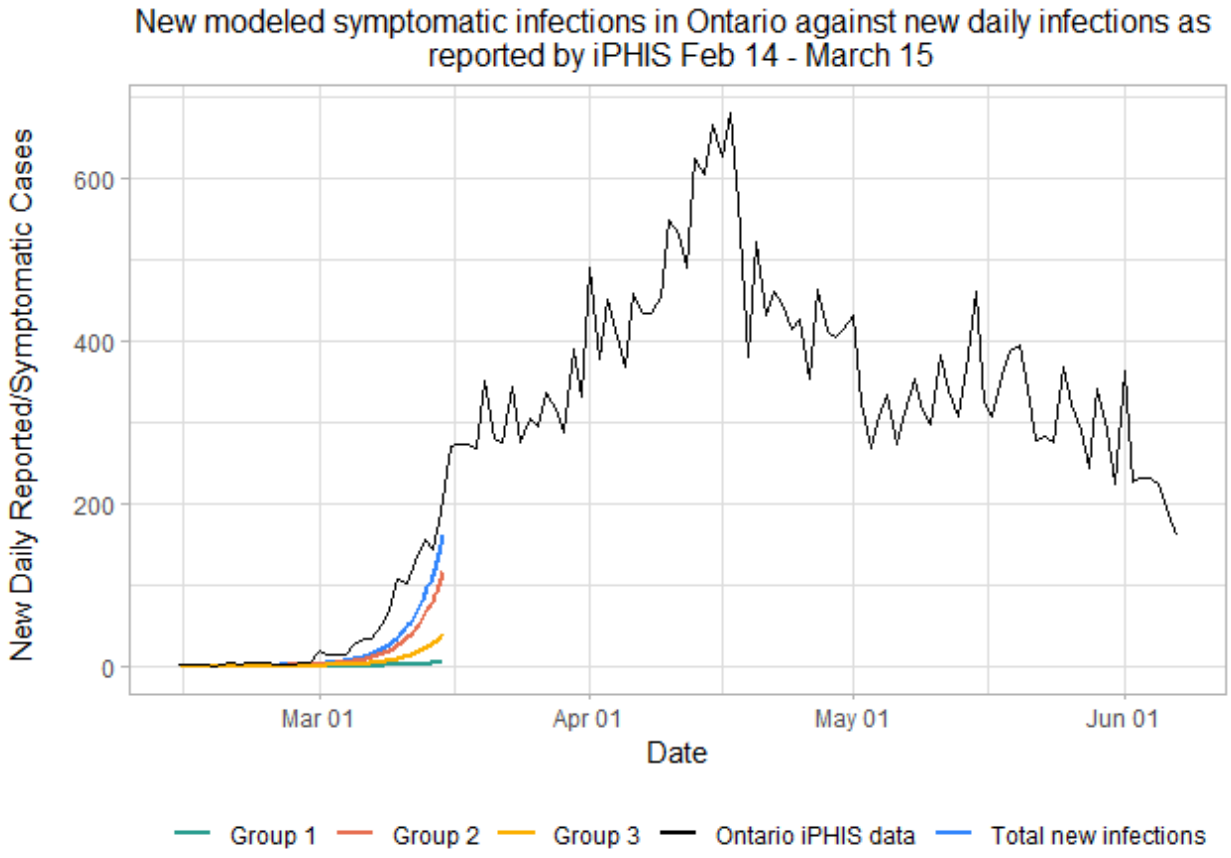

Figure 3.2: iPHIS data (black) and simulated pre-lockdown symptomatic infections in each of the 3 groups. The blue curve represents symptomatic infected in the overall Ontario population.

$p = 0.045085$. We solve for q_{int} and obtain the results in Figure 3.3.

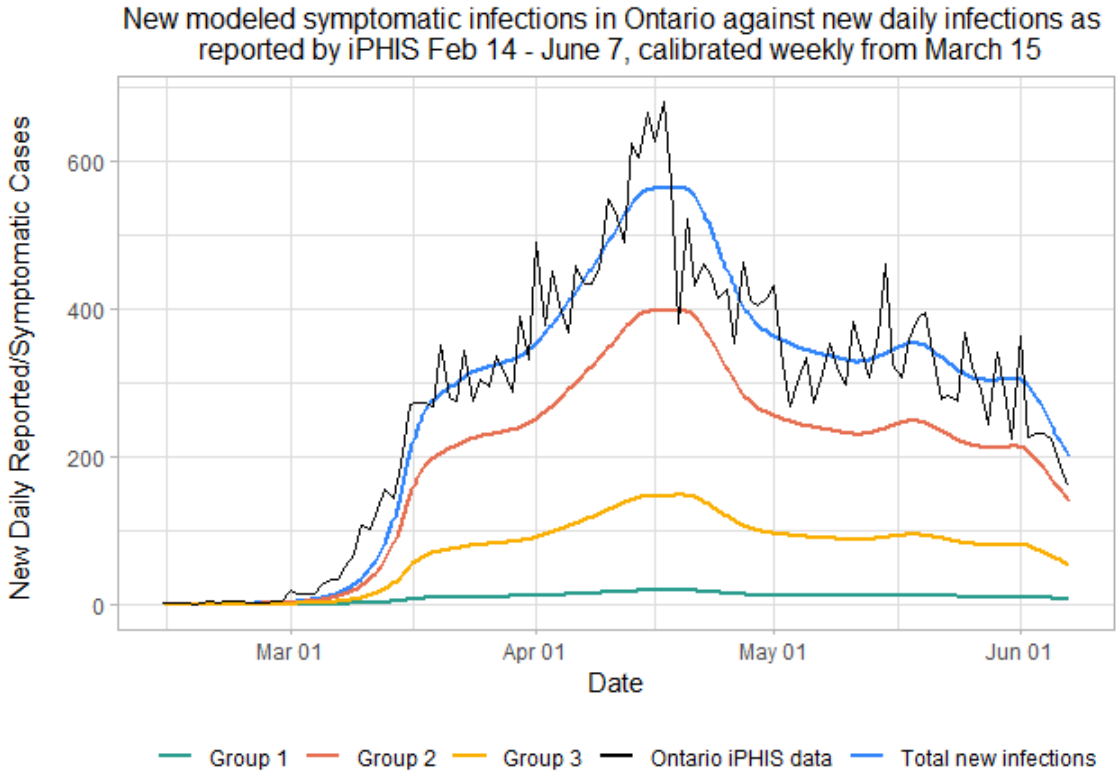

Figure 3.3: Simulated new daily symptomatic infections in each of the 3 age groups according to the SEILR(pas) model.

Recently, Google has released data for phone mobility in various countries around the world, compared to baseline, sorted by region and mobility type. Let us now consider M_{int}, average mobility during interval *int* compared to baseline, as our relative number of total contacts as compared to baseline. Thus, q no longer needs to account for mobility changes, and we introduce a new variable $\hat{q}$ to account for changes in transmissibility. Thus, when including mobility data,

$$q_{int} = M_{int} \cdot \hat{q}_{int}. \tag{3.3}$$

and thus

$$\beta_{ij}(int) = c_{ij} \cdot p \cdot M_{int} \cdot \hat{q}_{ij}, \quad \forall\ int \in interval. \tag{3.4}$$

The Golden Search Method for Minimizing SSE

With or without mobility, using our above model, we are left simulating a system of equations depending on a scalar unknown variable (either q or $\hat{q}$). The values of this variable change over time due to behavioural changes (e.g. mobility, mask wearing, maintaining physical distance, etc.). However, we can compute the optimal value of q or $\hat{q}$ over given intervals such that our simulated infected symptomatic curve in Ontario (adding the 3 groups) best matches the curve of onset COVID-19 cases in Ontario:

$$I^S_{new}(int) = \sum_{i=1}^{3} \alpha\psi I^P_i(int-1) \tag{3.5}$$

We solve for the optimal value of q during a preset time interval in such a way as to minimize the sum of squared errors (SSE) between $I^S_{new}(int)$ and the new daily reported cases from iPHIS. We begin this with int 0 =[Feb 14, Mar 14] as defined previously. Then due to the variable nature of new cases in Ontario after March 15, weekly time intervals are defined as before:

- int 0 := [Feb 14, Mar 14] (pre-lockdown)
- int i := [Mar 15+7(i-1), Mar 15 + 7i] or the ceiling of the i^{th} week following March 15

To minimize the SSE as described, we use the Golden Section Search algorithm, taking 2 initial approximate points for q or $\hat{q}$ and converging onto the local minimum in between the 2 points. To find the SSE, we compute

$$\text{Total New Symptomatic Infections in Ontario (TNSI)} = \sum_{1}^{interval} ((\sum_{n=1}^{K} \alpha \cdot \psi \cdot I^P_i(int-1)))$$

from our model on day t, and compare them to numbers reported by iPHIS.

$$SSE = ((\sum_{n=1}^{K} \alpha \cdot \psi \cdot I_i^P(int-1)) - iPHIS(int))^2 \tag{3.6}$$

$$\text{Standard Deviation } = \sqrt{\frac{(TNSI - iPHIS(int))^2}{interval}}. \tag{3.7}$$

Finally, we need to be mindful of the limitations of SEIR-type models to carefully trace delays between various stages of exposed, presymptomatic, etc. As such, a matching delay for q must be introduced before running the model. The optimal delay value was found to be 2 days, as described in sec:appendix2 of the Appendix.

3.2.6 SEILR(pas) model results

As shown in Figures 3.4 and 3.5, while Group 1 cases are modelled quite accurately, we under-predict cases in the senior population (Group 3), and over predict cases in adults (Group 2). This is especially true during the peak of this first wave, from the third to the sixth week following the initiation of lockdown, corresponding to March 29th to April 19th. During this time period, there were many outbreaks reported in Long Term Care (LTC) facilities in Ontario, putting the senior population at a disproportionately higher risk than usual [118].

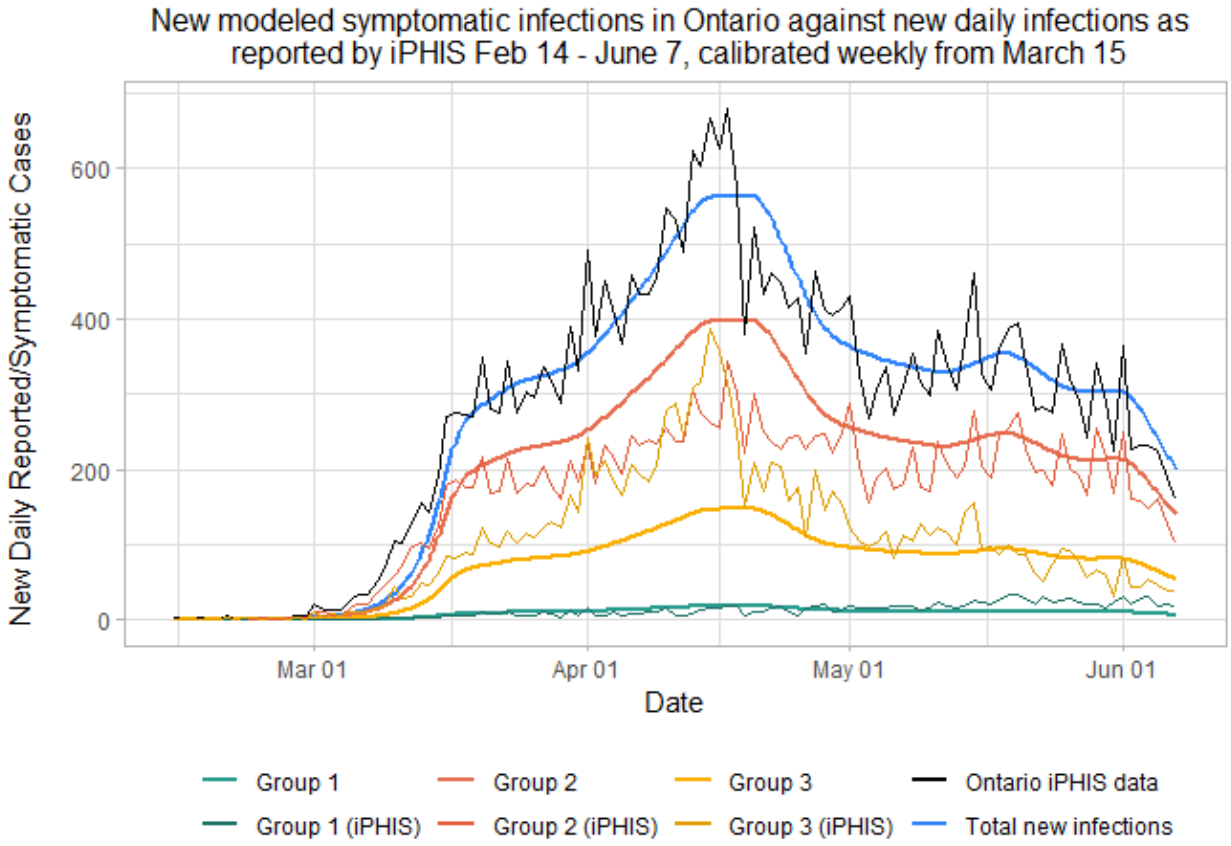

Figure 3.4: Simulated new daily symptomatic infections in each of the 3 age groups compared with iPHIS reported cases, stratified by age.

[rotate = 175, radius=3, color=green!50, red!60, yellow!70, text=legend] 4.22/Group 1 (iPHIS), 58.26/Group 2 (iPHIS), 37.52/Group 3 (iPHIS)
[rotate = 175, radius=3, color=green!50, red!60, yellow!70,text = legend] 3.24/Group 1 (modelled), 70.64/Group 2 (modelled), 26.12/Group 3 (modelled)

Figure 3.5: Proportion of COVID-19 cases in Ontario attributed to each age group for the real iPHIS reported numbers (top; total = 32,095, Group 1 = 1,336, Group 2 = 18,595, Group 3 = 12,004) vs. the SEILR(pas) model (bottom; total = 31,722, Group 1 = 1,029, Group 2 = 22,407, Group 3 = 8,286).

3.3 Results & Discussion

3.3.1 Removing outbreaks to match age-specific case rates

Infection in our model is governed by our contact patterns and our contact scaling through lockdown. Our model takes a very macroscopic approach to transmission, and does not consider smaller clusters of individuals and "superspreaders". As such, cases resulting from isolated outbreaks in long-term care homes, retirement homes, hospitals, group homes, shelters, and correctional facilities that occur as a result of close proximity are not accounted for by our model. During the first wave, iPHIS labeled such cases under the same umbrella term "outbreak" cases. We subsequently removed them from the data and re-ran the model to track only community contacts. Figures 3.6 and 3.7 show that when removing outbreak-related cases, we yield a much better match for age proportional case rates. Here, we match cases in Group 2 almost perfectly, while slightly over-predicting cases in seniors, and under-predicting cases in under-20s. This under-prediction in cases in young people can be accounted by the fact that our model does not include household transmission rates, which have been found to be much higher than external community transmission rates [119]. Since the vast majority of individuals under 20 years old live alongside adults, they inherit a higher risk than just through community transmission. The over-prediction in seniors can be attributed to the large numbers of seniors living in long-term care (LTC) facilities. Since all cases in LTC facilities are labeled 'outbreak', some seniors who may have gotten sick through external sources may have been labeled as 'outbreak' cases by iPHIS regardless. Thus, the outbreak-removed iPHIS data may be slightly under-representing non-outbreak cases in seniors.

Note that while the *total* cases differ between the models with outbreaks included versus removed, the relative *proportion* of cases for each age group remains consistent. This is to be expected, as the model has not been altered, it simply fits q to match to a different total

case number. Removing outbreaks has a significant impact on the age distribution of cases in iPHIS reported data, since outbreaks in LTC facilities disproportionately affect seniors [118].

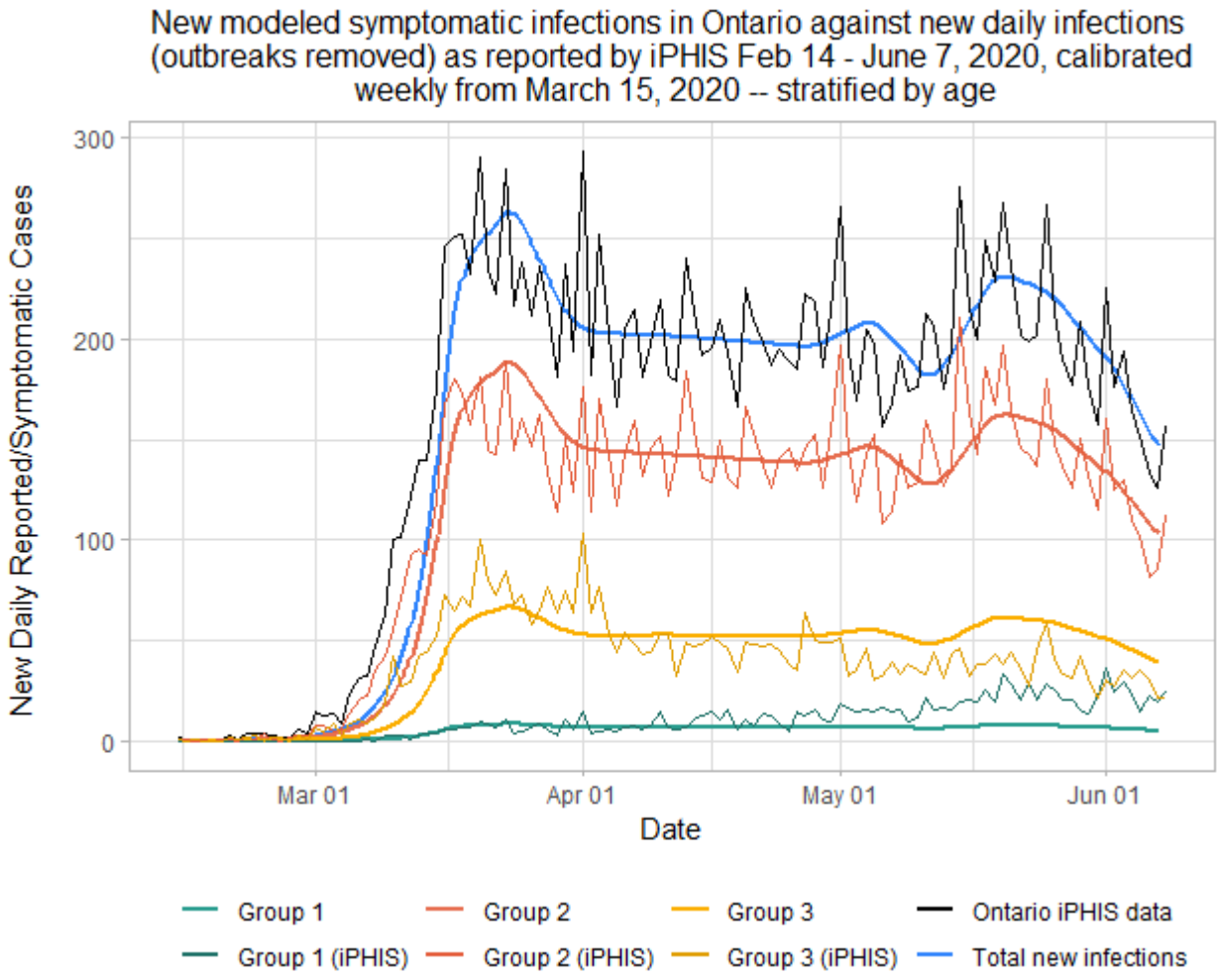

Figure 3.6: Simulated new daily symptomatic infections in each of the 3 age groups compared with iPHIS reported cases, stratified by age, **with outbreaks removed**.

[rotate = 165, radius=3, color=green!50, red!60, yellow!70, text=legend] 6.56/Group 1 (iPHIS), 69.76/Group 2 (iPHIS), 23.68/Group 3 (iPHIS)
[rotate = 175, radius=3, color=green!50, red!60, yellow!70,text = legend] 3.24/Group 1 (modelled), 70.64/Group 2 (modelled), 26.12/Group 3 (modelled)

Figure 3.7: Proportion of COVID-19 cases in Ontario attributed to each age group **with outbreaks removed** for the real iPHIS reported numbers (top; total = 18,614, Group 1 = 1,222, Group 2 = 12,985, Group 3 = 4,407) vs. the SEILR(pas) model (bottom; total = 17,970, Group 1 = 582, Group 2 = 12,705, Group 3 = 4,683).

3.3.2 Estimates of mobility and behaviour during the pandemic's first wave

To better understand the behaviour of the epidemic curve as influenced by mobility reductions, contact reductions, and other NPIs, we first estimate R_0, the basic reproductive number of the virus near the disease-free equilibrium (pre-lockdown). To determine R_0 using our model, we compute the spectral radius of the next generation matrix from the Jacobian of our model equations in Section 3.2.1, assuming a pre-lockdown value of $q = 1$. Doing so yields $R_0 = 5.88$ during this pre-lockdown phase. Then we look to find a value for our parameter q that would cause no new growth in daily case numbers after lockdown, once the first wave began to take hold. Because the population is no longer fully susceptible, we now calculate R_e. Specifically,

$$R_e = R_0 \times \frac{S(t)}{S(0)}$$

Typically, R_0 is dependent on the value of β, which we have defined as dependent on q, making R_e also dependent on q. We then use the expression

$$R_e = R_0 \times q \times \frac{S(t)}{S(0)}$$

so that we can determine R_e at any point during our timeline.

With the addition of q, we apply the same calculation as before and find that with

$p = 0.045$ and $q = 0.17$, $R_e \approx 1$. This implies that 0.17 is our threshold value for q, denoted $\bar{q}$, that prevents total new cases from increasing. [3] At q values above this threshold we expect the cases to increase, and at q values below this threshold we expect case numbers to decrease over time. For this reason, it is interesting to investigate the behaviour of q over time (Figure 3.8).

When comparing the placement of q relative to $\bar{q}$ to the behaviour of disease spread over the same time intervals, it can be observed that when $q < \bar{q}$, case numbers decrease, when $q > \bar{q}$, case numbers rise, and when $q \approx \bar{q}$, case numbers remain relatively consistent. When we introduce Google mobility data to the model, the resulting epidemic curve is nearly identical to the model that did not utilize Google mobility. This is to be expected, as $q_{int} = M_{int} \cdot \hat{q}_{int}$, allowing $\beta_{ij\ int}$ to remain consistent between the two models. When overlaying the graphs, this is even more evident (see Figure 3.9).

It is interesting to investigate how $\hat{q}$ and M change relative to q (Figure 3.10). As expected, both M and $\hat{q}$ drop significantly as soon as lockdown measures are implemented. When comparing q to changes in Google mobility, the change vs. baseline is quite different in shape, with the exception of the initial drop in both. While mobility slowly rises over time, q slowly falls. This does not suggest that mobility is completely unassociated with q, simply that it is not necessary to keep mobility exceedingly low in order to keep q low as long as other precautionary measures are taken.

[3] We investigated changes in threshold values of q when we half the compliance rate ϵ, or when we double or quadruple the isolation rate $k \in \{2, 4\}$, respectively. We registered extremely small variations in the threshold q-values, within the 0.17 ± 10^{-2} magnitude.

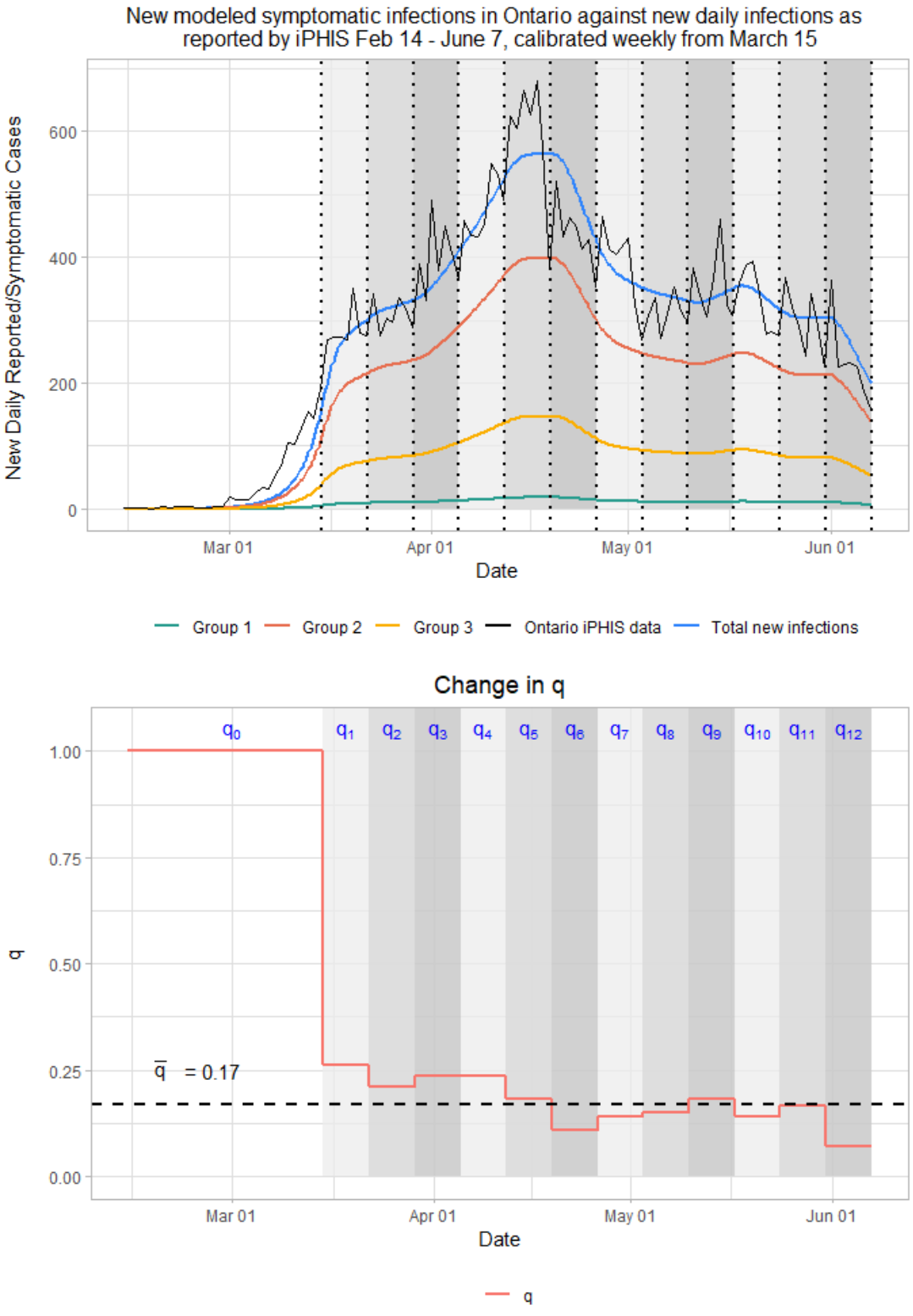

Figure 3.8: Change in q over time as compared to threshold, $\bar{q} = 0.17$.

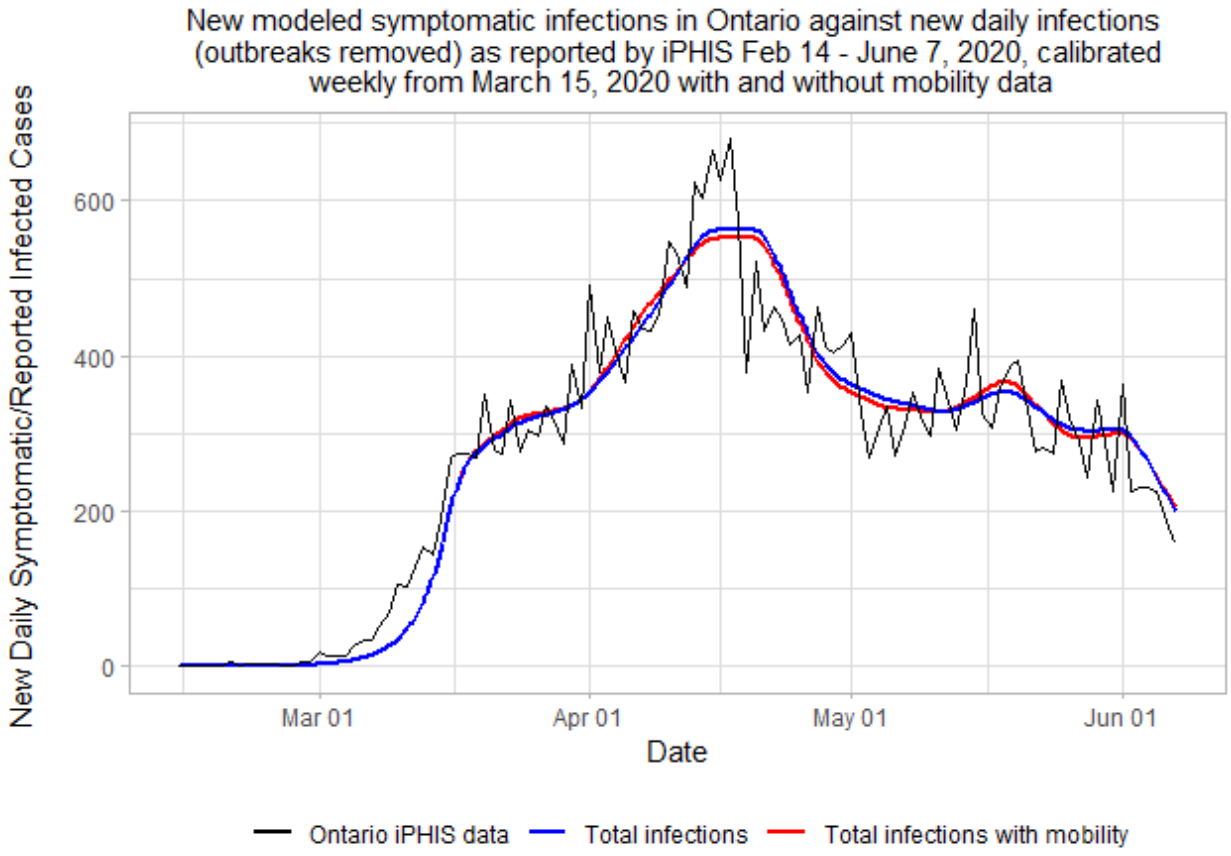

Figure 3.9: Comparison of SEILR(pas) model epidemic curves, with and without mobility data.

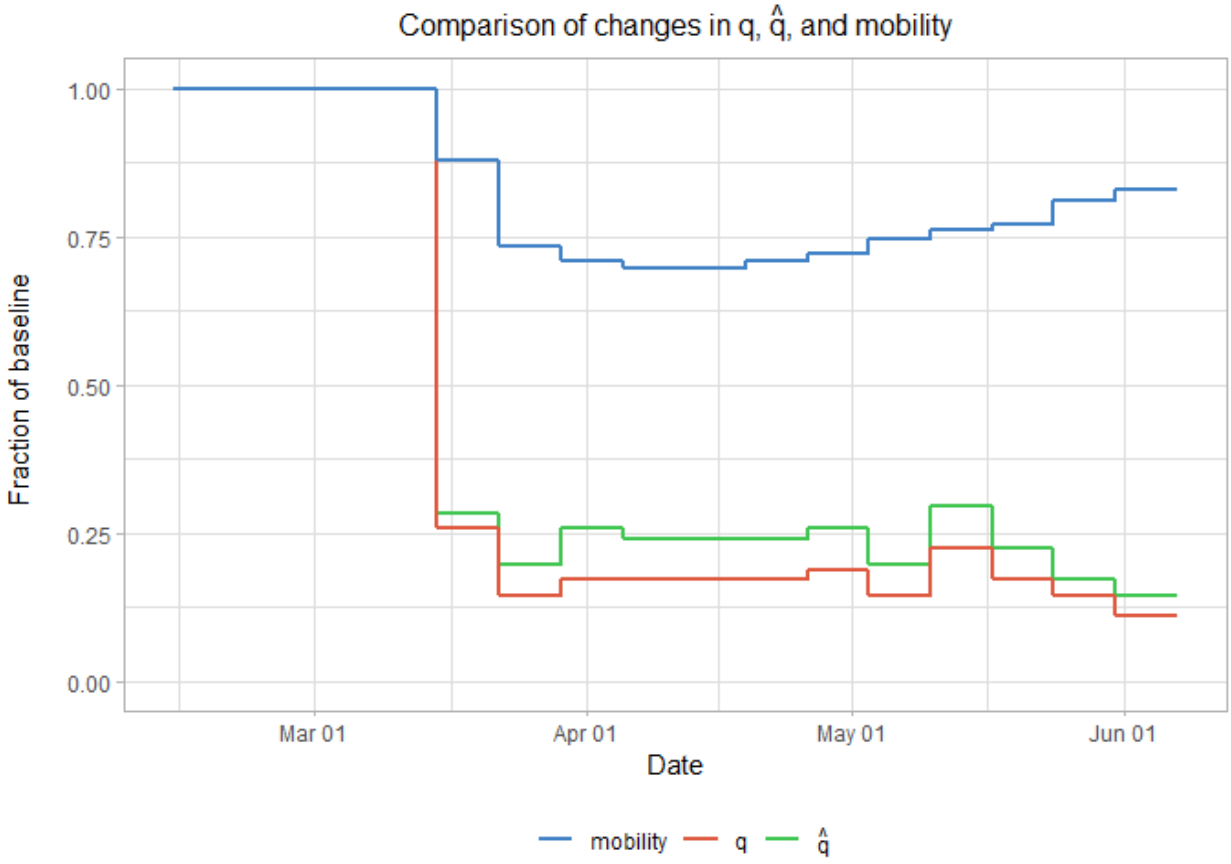

Figure 3.10: Relative changes in mobility data, the transmission scaling factor (q), and the the transmission scaling factor decoupled from mobility data ($\hat{q}$) from February 14 - June 7.

Conversely, when comparing q to $\hat{q}$, one notices they are actually very similar shape, just with $\hat{q}$ behaving with more drastic increases and decreases. This is because the dampening effect of $\hat{q}$ on transmission is amplified by the additional dampening effect of mobility ($\sim$0.5), and so q must dampen $\sim$twice as much in order to yield a similar effect in each β_{ij} (recall that $q = M \cdot \hat{q}$). This is exemplified towards the end of the model as mobility begins to trend back towards baseline, causing $\hat{q}$ to trend closer to q. The closer mobility gets to 1, the less of an effect it has keeping effective contacts low, and so the more that one can attribute the decrease in disease transmission to external factors.

The value of q is quite well behaved, dropping to roughly 25% of baseline immediately following implementation of COVID-19 measures, and staying relatively stable in the time following. Mobility also drops following these implementations, though slightly more slowly, and only to about 70% of baseline, before slowly creeping above 80% by the end of the model (June 7th). Interestingly, from *int* 4 (March 30 - April 6) to *int* 5 (April 6 - April 13) while Google mobility and $\hat{q}$ vary slightly, their relative changes cancel out such that q stays the same at 16.99% of baseline, very slightly below our $\bar{q} = 0.17$. During this time, case numbers remain almost completely stable, just slightly increasing over time as we are slightly below our threshold. Additionally, as more people are infected and recover from the virus, the proportion of individuals within the Susceptible compartment decreases, lowering R_e as well. With case numbers as low as they are for the time period modeled, this has a very small impact on the model as as whole.

The epidemic curve resulting from using outbreak-removed data (Figure 3.6) is significantly flatter and more consistently behaved than the curve that included highly localized outbreaks (Figure 3.4). Other than a small spike during the initial week following lockdown, and a second peak towards the end of May, new cases were consistent at approximately 200 per day. Even during the two peaks, cases never exceeded 300 new cases in a day in either the iPHIS or modeled data. This is in stark contrast to the previous iteration of the model

in Section 2 that included outbreak-related cases, as case number surges and drop-offs are now comparatively stable. This suggests that community transmission in Ontario during our time period is relatively consistent and predictable over time, while the majority of surges are due to localized outbreaks. The community has been able to keep cases numbers consistent as well, suggesting a overall R_e value of approximately 1 given the guidelines and protocols established provincially. This is even more evident when examining the q plot (Figure 3.11).

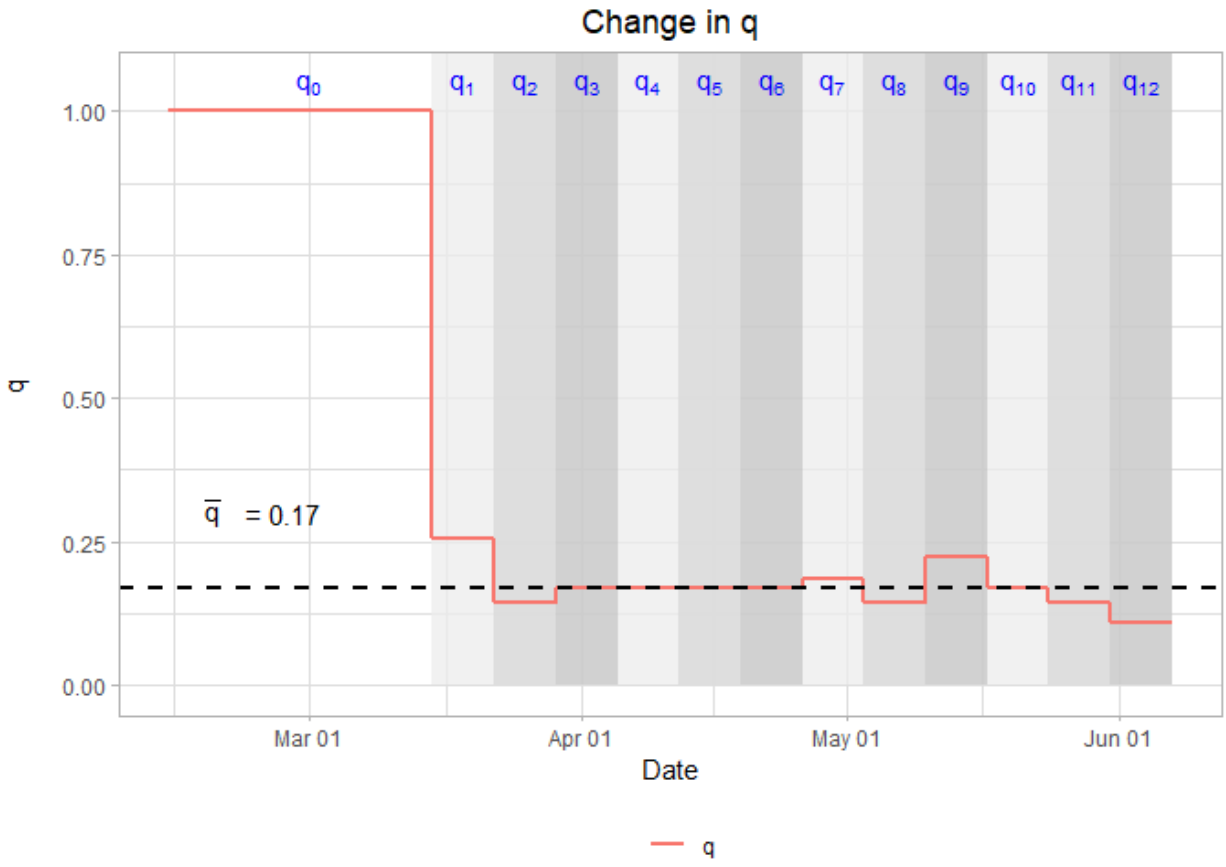

Figure 3.11: Change in q over time with outbreak cases removed as compared to threshold $\bar{q} = 0.17$.

From *int* 1 through *int* 12, $q \in [0.1101416, 0.2565002]$. This yields an $R_e \in [0.6487918, 1.5058941]$, with an overall average of $R_{eff\ avg} = 1.007796$ during this time period. This shows that Ontario communities are living in a delicate balance, very close to

an $R_e = 1$. This suggests that even a relatively minor shift in behaviour (distancing, mask wearing, mobility, etc.) that increases our R_e can easily result in further eclipsing $R_e = 1$, and will lead to more significant growth in case numbers over time.

3.4 Limitations and further work

There are some limitations to the work presented here. First, our model assumes uniform transmissibility, uniform susceptibility, and uniform contact dampening as a result of lockdown across the three age groups, which may not be true [120, 121, 122]. As well, our model only considers a period of time when non-pharmaceutical interventions (NPIs) were used to mitigate infection spread (e.g. no vaccinations). Now that the pandemic is much further along, different parameters may be established at new time points to reflect newly instated measures of control in our model. Additionally, when we employ the outbreaks-removed data to find a better fit for our model, we do not make adjustments to our assumed population sizes. As there are a wide range of definitions for potential outbreak locations, we cannot know from which age subgroup outbreak cases are removed.

- population remains constant when including OB to when removing OB because we don't know "who" the OB population are (they could come from any category), since there are a wide range of definitions for potential outbreak locations, and we don't know their respective demographics

- now that the pandemic is much further along, we may incorporate new parameters at new time points to reflect newly instated measures of control in our model

- our model assumes uniform transmissibility, uniform susceptibility, and uniform contact dampening as a result of lockdown across the three age groups, which may not be true [120, 121, 122]

3.5 Conclusion

Using our SEILR(pas) model in conjunction with Canadian contact rates and mobility data, we have successfully modeled new daily Ontario cases from February 14 to June 7, 2020 while matching age-specific case rates. We accomplish this by tracking the dampening effects of preventative measures, represented by variable q. When removing cases associated with localized outbreaks, we observe that the vast majority of variability in new cases is a result of these outbreaks. When considering community transmission only, Ontario has generally maintained an $R_e \approx 1$ over the course of our modeled time period. This suggests that even a slight change that results in increasing R_e can result in daily case numbers growing over time, rather than remaining stable or decreasing as was the case towards the end of June. When considering changes in mobility, we find that while mobility has increased towards the end of our time period, preventative measures such as hand-washing, physical distancing, and mask-wearing have been sufficient to maintain an $R_e \approx 1$. It is important to note that using the mobility reduction as a signal for pandemic evolution is not easy, nor perhaps desirable, especially in a simple model such as this. We clearly see that a large suppression of mobility has helped arrest the spread, however that level is generally unsustainable beyond a few weeks and mobility will invariably be pushed back up towards baseline values over time. Disentangling mobility reduction in contacts from other NPI measures reduction teaches us that the collective impact of NPIs are perhaps a better representation for the evolution of the Ontario pandemic in the time frame considered.

We also found that the contact rates provided by Prem, Cook, & Jit (2017) [86] in combination with the age-specific symptomatic rates provided by Davies et al. (2020) [84] resulted in closely matching proportions for working-age populations and senior populations, but underestimated cases in young people. This is likely due to a combination of the effects of household transmission, differing degrees of susceptibility and transmissibility between age

groups, differing responses to lockdown between age groups [120], and differing likelihoods to receive testing between age groups. This can be fixed in the future, however it would require more complete data. The lack of testing before lockdown is implemented precludes us from accurately assessing differences in susceptibility decoupled from mobility.

Chapter 4

Concluding remarks

This work demonstrates that public uptake of a particular program or practice plays a large role in the development and success of health interventions against human morbidity and mortality. Through optimization modeling, we were able to explore the trajectory and potential confounding impacts on the progression of disease response and management in Ontario for each an infectious and a non-infectious disease.

The stochastic dynamic programming approach used in Chapter 2 allowed for the monthly estimation of the existing level of population coverage against shingles, both in terms of vaccine courses distributed and effective protection conferred, due to the first publicly funded HZ immunization program in Ontario. Using this as a base case, the same model was applied with similar parameters for the allocation and budget forecast in the new program after 2020. This model would also allow for simulating scenarios with a larger window of eligibility that may improve quality of life for those who participated in the first program or are yet to receive a vaccine.

In Chapter 3, an SEIR compartmental model was used to track data changes on a much smaller time scale, offering a day-to-day visualization of the early stages of response to the COVID-19 pandemic in Ontario. Mobility was found not to play as large of a role as other

preventative measures, and the removal of local outbreak chains in LTC facilities clarified what the reproduction number for Ontario actually looked like during this time. Both factors elucidated the true impact of NPI measures in the province among different age groups from March to June 2020, and provided a more detailed account of infection spread during the first wave in Ontario.

Demonstrated in the chapters mentioned above, model frameworks and the nature of diseases may differ, but the conclusion is that opportunities should always be taken to reflect on the evolution of data and identify weaknesses or improvements. Pilot attempts will always require tweaking, and the use of optimization-based models like those presented here can provide a foundation for evaluation.

REFERENCES

[1] K. J. Friesen, D. Chateau, J. Falk, S. Alessi-Severini, and S. Bugden, "Cost of shingles: population based burden of disease analysis of herpes zoster and postherpetic neuralgia," *BMC infectious diseases*, vol. 17, no. 1, pp. 1–8, 2017.

[2] Government of Ontario, "Aging with confidence: Ontario's action plan for seniors," November 2017.

[3] Merck Frosst Canada Ltd., "Product monograph - Zostavax ii," 2018.

[4] GlaxoSmithKline Inc., "Product monograph including patient medication information - shingrix," 2017.

[5] *3.04 Immunization*, p. 155. Office of the Auditor General of Ontario, 2014.

[6] Public Health Agency of Canada, "Vaccine uptake in Canadian adults: Results from the 2016 Adult National Immunization Coverage Survey (anics)," tech. rep., Public Health Agency of Canada, 2018.

[7] V. Rémy, Y. Zöllner, and U. Heckmann, "Vaccination: the cornerstone of an efficient healthcare system," *Journal of market access & health policy*, vol. 3, no. 1, p. 27041, 2015.

[8] M. Shapiro, B. Kvern, P. Watson, L. Guenther, J. McElhaney, and A. McGeer, "Update on herpes zoster vaccination: a family practitioner's guide," *Canadian Family Physician*, vol. 57, no. 10, pp. 1127–1131, 2011.

[9] R. Bellman, "Dynamic programming," *Science*, vol. 153, no. 3731, pp. 34–37, 1966.

[10] J. Fang, L. Zhao, J. C. Fransoo, and T. Van Woensel, "Sourcing strategies in supply risk management: An approximate dynamic programming approach," *Computers & Operations Research*, vol. 40, no. 5, pp. 1371–1382, 2013.

[11] J. G. Dai and P. Shi, "Inpatient overflow: An approximate dynamic programming approach," *Manufacturing & Service Operations Management*, vol. 21, no. 4, pp. 894–911, 2019.

[12] N. Geng, X. Xie, and Z. Zhang, "Addressing healthcare operational deficiencies using stochastic and dynamic programming," *International Journal of Production Research*, vol. 57, no. 14, pp. 4371–4390, 2019.

[13] H. W. Hethcote and P. Waltman, "Optimal vaccination schedules in a deterministic epidemic model," *Mathematical Biosciences*, vol. 18, no. 3-4, pp. 365–381, 1973.

[14] M. W. Tanner, L. Sattenspiel, and L. Ntaimo, "Finding optimal vaccination strategies under parameter uncertainty using stochastic programming," *Mathematical biosciences*, vol. 215, no. 2, pp. 144–151, 2008.

[15] O. Y. Özaltın, O. A. Prokopyev, A. J. Schaefer, and M. S. Roberts, "Optimizing the societal benefits of the annual influenza vaccine: A stochastic programming approach," *Operations research*, vol. 59, no. 5, pp. 1131–1143, 2011.

[16] J. T. Wu, L. M. Wein, and A. S. Perelson, "Optimization of influenza vaccine selection," *Operations Research*, vol. 53, no. 3, pp. 456–476, 2005.

[17] M. Harvey, B. Denton, L. Prosser, and D. Hutton, "Determining the optimal strategy for the live-attenuated herpes zoster vaccine in adults," *Vaccine*, vol. 36, no. 41, pp. 6237–6247, 2018.

[18] G. Amirthalingam, N. Andrews, P. Keel, D. Mullett, A. Correa, S. de Lusignan, and M. Ramsay, "Evaluation of the effect of the herpes zoster vaccination programme 3 years after its introduction in England: a population-based study," *The Lancet Public Health*, vol. 3, no. 2, pp. e82–e90, 2018.

[19] N. Andrews, J. Stowe, G. Kuyumdzhieva, B. Sile, I. Yonova, S. de Lusignan, M. Ramsay, and G. Amirthalingam, "Impact of the herpes zoster vaccination programme on hospitalised and general practice consulted herpes zoster in the 5 years after its introduction in England: a population-based study," *BMJ open*, vol. 10, no. 7, p. e037458, 2020.

[20] J. Lin, J. G. Wood, C. Bernardo, N. P. Stocks, and B. Liu, "Herpes zoster vaccine coverage in Australia before and after introduction of a national vaccination program," *Vaccine*, vol. 38, no. 20, pp. 3646–3652, 2020.

[21] W. L. Winston and J. B. Goldberg, *Operations research: applications and algorithms*, vol. 3. Thomson/Brooks/Cole Belmont, 2004.

[22] Ministry of Health and Long-Term Care, "Publicly-funded shingles (herpes zoster) immunization program: Information for health care providers," 2016.

[23] Public Health Agency of Canada, "An Advisory Committee Statement (acs) National Advisory Committee on Immunization (NACI): Updated recommendations on the use of herpes zoster vaccines," tech. rep., Public Health Agency of Canada, 2018.

[24] P. E. Kilgore, D. Kruszon-Moran, J. F. Seward, A. Jumaan, F. P. Van Loon, B. Forghani, G. M. McQuillan, M. Wharton, L. J. Fehrs, C. K. Cossen, *et al.*, "Varicella in Americans from NHANES iii: implications for control through routine immunization," *Journal of medical virology*, vol. 70, no. S1, pp. S111–S118, 2003.

[25] D. W. Kimberlin and R. J. Whitley, "Varicella–zoster vaccine for the prevention of herpes zoster," *New England Journal of Medicine*, vol. 356, no. 13, pp. 1338–1343, 2007.

[26] M. N. Oxman, M. J. Levin, G. Johnson, K. Schmader, S. Straus, L. Gelb, R. Arbeit, M. Simberkoff, A. Gershon, L. Davis, *et al.*, "A vaccine to prevent herpes zoster and postherpetic neuralgia in older adults," *New England Journal of Medicine*, vol. 352, no. 22, pp. 2271–2284, 2005.

[27] R. Hope-Simpson, "Postherpetic neuralgia," *The Journal of the Royal College of General Practitioners*, vol. 25, no. 157, pp. 571–575, 1975.

[28] R. H. Dworkin and R. K. Portenoy, "Pain and its persistence in herpes zoster," *Pain*, vol. 67, no. 2-3, pp. 241–251, 1996.

[29] R. W. Johnson and R. H. Dworkin, "Treatment of herpes zoster and postherpetic neuralgia," *Bmj*, vol. 326, no. 7392, pp. 748–750, 2003.

[30] M. Brisson, J. M. Pellissier, S. Camden, C. Quach, and P. De Wals, "The potential cost-effectiveness of vaccination against herpes zoster and post-herpetic neuralgia," *Human vaccines*, vol. 4, no. 3, pp. 238–245, 2008.

[31] R. Warrington and S. Ismail, "Summary of the NACI update on herpes zoster vaccines," *Canada Communicable Disease Report*, vol. 44-9, pp. 220–225, September 2018.

[32] Government of Ontario, "Ontario making shingles vaccine free for seniors," September 2016.

[33] Ministry of Health, "Transition to publicly funded Shingrix® vaccine for Ontario's shingles (herpes zoster) immunization program: Information for health care providers," 2020.

[34] Public Health Agency of Canada, "Vaccine uptake in Canadian Adults 2019," 2019.

[35] B. M. McDonald, D. C. Dover, K. A. Simmonds, C. A. Bell, L. W. Svenson, and M. L. Russell, "The effectiveness of shingles vaccine among Albertans aged 50 years or older: A retrospective cohort study," *Vaccine*, vol. 35, no. 50, pp. 6984–6989, 2017.

[36] K. Dooling, A. Guo, M. Patel, *et al.*, "Morbidity and mortality weekly report recommendations of the advisory committee on immunization practices for use of herpes zoster vaccines," *Morbidity and Mortality Weekly Report*, vol. 67, 2018.

[37] B. J. Skinner, "Vaccines policy in Canada: International and domestic comparisons," 2020.

[38] Ontario Ministry of Health and Long-Term Care, "Ontario publicly funded shingles (herpes zoster) immunization program: Shingrix vaccine information for patients," 2020.

[39] Statistics Canada, "Table: 17-10-0009-01: Population estimates, quarterly," 2021.

[40] P. T. de Boer, A. van Lier, H. de Melker, A. J. van Wijck, J. C. Wilschut, A. J. van Hoek, and M. J. Postma, "Cost-effectiveness of vaccination of immunocompetent older adults against herpes zoster in the Netherlands: a comparison between the adjuvanted subunit and live-attenuated vaccines," *BMC medicine*, vol. 16, no. 1, pp. 1–18, 2018.

[41] P. Le and M. B. Rothberg, "Cost-effectiveness of the adjuvanted herpes zoster subunit vaccine in older adults," *JAMA internal medicine*, vol. 178, no. 2, pp. 248–258, 2018.

[42] D. Martins, D. McCormack, M. Tadrous, T. Gomes, J. C. Kwong, M. M. Mamdani, S. A. Buchan, and T. Antoniou, "Impact of a publicly funded herpes zoster immunization program on the burden of disease in Ontario, Canada: A population-based study," *Clinical Infectious Diseases*, vol. 72, no. 2, pp. 279–284, 2021.

[43] W. W. Williams, P.-J. Lu, A. O'Halloran, D. K. Kim, L. A. Grohskopf, T. Pilishvili, T. H. Skoff, N. P. Nelson, R. Harpaz, L. E. Markowitz, *et al.*, "Surveillance of vaccination coverage among adult populations—United States, 2014," *Morbidity and Mortality Weekly Report: Surveillance Summaries*, vol. 65, no. 1, pp. 1–36, 2016.

[44] C. for Disease Control, Prevention, *et al.*, "Vaccination coverage among adults in the United States, National Health Interview Survey, 2016," *National Center for Immunization and respiratory diseases*, 2018.

[45] Centers for Disease Control and Prevention, "2018 adult vaccination coverage general population report - pneumococcal vaccination coverage among adults 18-64 years at increased risk and $\geq$ 65 years, Td and Tdap vaccination coverage among adults 18 years, and shingles vaccination among adults 60 years, by state, HHS region, and the United States, brfss, 2018," 2020.

[46] R. C. Hechter, S. Y. Tartof, S. J. Jacobsen, N. Smith, and H. F. Tseng, "Trends and disparity in zoster vaccine uptake in a managed care population," *Vaccine*, vol. 31, no. 41, pp. 4564–4568, 2013.

[47] H. Lal, A. L. Cunningham, O. Godeaux, R. Chlibek, J. Diez-Domingo, S.-J. Hwang, M. J. Levin, J. E. McElhaney, A. Poder, J. Puig-Barberà, *et al.*, "Efficacy of an adjuvanted herpes zoster subunit vaccine in older adults," *New England Journal of Medicine*, vol. 372, no. 22, pp. 2087–2096, 2015.

[48] A. L. Cunningham, H. Lal, M. Kovac, R. Chlibek, S.-J. Hwang, J. Díez-Domingo, O. Godeaux, M. J. Levin, J. E. McElhaney, J. Puig-Barberà, *et al.*, "Efficacy of the herpes zoster subunit vaccine in adults 70 years of age or older," *New England Journal of Medicine*, vol. 375, no. 11, pp. 1019–1032, 2016.

[49] R. Chlibek, J. Smetana, K. Pauksens, L. Rombo, J. A. R. Van den Hoek, J. H. Richardus, G. Plassmann, T. F. Schwarz, E. Ledent, and T. C. Heineman, "Safety and immunogenicity of three different formulations of an adjuvanted varicella-zoster virus subunit candidate vaccine in older adults: a phase ii, randomized, controlled study," *Vaccine*, vol. 32, no. 15, pp. 1745–1753, 2014.

[50] L. Chen, W. Liu, Q. Zhang, K. Xu, G. Ye, W. Wu, Z. Sun, F. Liu, K. Wu, B. Zhong, Y. Mei, W. Zhang, Y. Chen, Y. Li, M. Shi, K. Lan, and Y. Liu, "RNA based mNGS approach identifies a novel human coronavirus from two individual pneumonia cases in 2019 Wuhan outbreak," *Emerging Microbes & Infections*, vol. 9, no. 1, pp. 313–319, 2020. PMID: 32020836.

[51] "COVID-19 Dashboard by the Center for Systems Science and Engineering (CSSE) at Johns Hopkins University (JHU)."

[52] I. Holmdahl and C. Buckee, "Wrong but useful—what COVID-19 epidemiologic models can and cannot tell us," *New England Journal of Medicine*, vol. 383, no. 4, pp. 303–305, 2020.

[53] L. P. James, J. A. Salomon, C. O. Buckee, and N. A. Menzies, "The use and misuse of mathematical modeling for infectious disease policymaking: Lessons for the COVID-19 pandemic," *Medical Decision Making*, p. 0272989X21990391, 2021.

[54] D. Adam, "Special report: The simulations driving the world's response to COVID-19.," *Nature*, vol. 580, no. 7803, p. 316, 2020.

[55] G. W. Leibniz, "1684. nova methodus pro maximis et minimis, itemque tangentibus, quae nec fractas, nec irrationales quantitates moratur, et singulare pro illis calculi genus," *Acta eruditorum*, pp. 467–473, 1859.

[56] G. W. Leibniz, "De geometria recondita et analysi indivisibilium atque infinitorum," *Acta eruditorum*, vol. 5, no. 1686, pp. 281–282, 1863.

[57] G. W. Leibniz, "Supplementum geometriae dimensoriae seu generalissima omnium tetragonismorum effectio per motum: similiterque multiplex constructio lineae ex data tangentium conditione," *Acta eruditorum*, vol. 12, no. 1693, pp. 385–392.

[58] J. Bernoulli, "Explicationes, annotationes & additiones ad ea, quae in actis sup. de curva elastica, isochrona paracentrica, & velaria, hinc inde memorata, & paratim controversa legundur; ubi de linea mediarum directionum, alliisque novis," *Acta Eruditorum*, vol. 1695.

[59] D. Bernoulli and S. Blower, "An attempt at a new analysis of the mortality caused by smallpox and of the advantages of inoculation to prevent it," *Reviews in medical virology*, vol. 14, no. 5, p. 275, 2004.

[60] W. Farr, "On the cattle plague," *J. Soc. Sci*, vol. 1, no. 7, pp. 349–351, 1866.

[61] D. Lilienfeld, "Celebration: William Farr (1807–1883)—an appreciation on the 200th anniversary of his birth," *International journal of epidemiology*, vol. 36, no. 5, pp. 985–987, 2007.

[62] G. Evans, "On some arithmetical questions involved in the rise and progress of epidemics," *Transactions. Epidemiological Society of London*, vol. 3, no. Pt 3, p. 551, 1876.

[63] J. Brownlee, "Investigations into the periodicity of infectious diseases by the application of a method hitherto only used in physics," *Public Health*, vol. 28, no. 4, pp. 125–134, 1915.

[64] J. Brownlee, "On the curve of the epidemic," *British Medical Journal*, vol. 2, no. 2900, pp. 142–, 1916.

[65] R. Ross, "An application of the theory of probabilities to the study of a priori pathometry.—part i," *Proceedings of the Royal Society of London. Series A, Containing papers of a mathematical and physical character*, vol. 92, no. 638, pp. 204–230, 1916.

[66] R. Ross and H. P. Hudson, "An application of the theory of probabilities to the study of a priori pathometry.—part ii," *Proceedings of the Royal Society of London. Series A, Containing papers of a mathematical and physical character*, vol. 93, no. 650, pp. 212–225, 1917.

[67] R. Ross and H. P. Hudson, "An application of the theory of probabilities to the study of a priori pathometry.–part iii," *Proceedings of the Royal Society of London. Series B, Containing papers of a biological character*, vol. 89, no. 621, pp. 507–507, 1917.

[68] W. O. Kermack and A. G. McKendrick, "A contribution to the mathematical theory of epidemics," *Proceedings of the Royal Society of London. Series A, Containing papers of a mathematical and physical character*, vol. 115, no. 772, pp. 700–721, 1927.

[69] J. Satsuma, R. Willox, A. Ramani, B. Grammaticos, and A. Carstea, "Extending the SIR epidemic model," *Physica A: Statistical Mechanics and its Applications*, vol. 336, no. 3-4, pp. 369–375, 2004.

[70] V. Capasso and G. Serio, "A generalization of the Kermack-McKendrick deterministic epidemic model," *Mathematical biosciences*, vol. 42, no. 1-2, pp. 43–61, 1978.

[71] M. Lavielle, M. Faron, J.-D. Zeitoun, *et al.*, "Extension of a sir model for modelling the propagation of COVID-19 in several countries.," *medRxiv*, 2020.

[72] F. Brauer, "Compartmental models in epidemiology," in *Mathematical epidemiology*, pp. 19–79, Springer, 2008.

[73] N. T. Bailey *et al.*, *The mathematical theory of infectious diseases and its applications*. Charles Griffin & Company Ltd, 5a Crendon Street, High Wycombe, Bucks HP13 6LE., 1975.

[74] C. Reveller, W. Lynn, and F. Feldmann, "An optimization model of tuberculosis epidemiology," *Management Science*, vol. 16, no. 4, pp. B–190, 1969.

[75] W. Zhang, W. G. W. Zhao, D. Wu, and Y. Yang, "Predicting COVID-19 trends in Canada: A tale of four models," *Cognitive Computation and Systems*, May 2020.

[76] L. Peng, W. Yang, D. Zhang, C. Zhuge, and L. Hong, "Epidemic analysis of COVID-19 in China by dynamical modeling," *arXiv preprint arXiv:2002.06563*, 2020.

[77] B. Tang, X. Wang, Q. Li, N. L. Bragazzi, S. Tang, Y. Xiao, and J. Wu, "Estimation of the transmission risk of the 2019-nCoV and its implication for public health interventions," *Journal of clinical medicine*, vol. 9, no. 2, p. 462, 2020.

[78] C. Hou, J. Chen, Y. Zhou, L. Hua, J. Yuan, S. He, Y. Guo, S. Zhang, Q. Jia, C. Zhao, *et al.*, "The effectiveness of quarantine of Wuhan city against the Corona Virus Disease 2019 (covid-19): A well-mixed seir model analysis," *Journal of medical virology*, 2020.

[79] L. López and X. Rodo, "A modified SEIR model to predict the COVID-19 outbreak in Spain and Italy: simulating control scenarios and multi-scale epidemics," *Available at SSRN 3576802*, 2020.

[80] J. Wu, B. Tang, N. L. Bragazzi, K. Nah, and Z. McCarthy, "Quantifying the role of social distancing, personal protection and case detection in mitigating COVID-19 outbreak in Ontario, Canada," *Journal of Mathematics in Industry*, vol. 10, May 2020.

[81] A. R. Tuite, D. N. Fisman, and A. L. Greer, "Mathematical modelling of COVID-19 transmission and mitigation strategies in the population of Ontario, Canada," *CMAJ*, vol. 192, no. 19, pp. E497–E505, 2020.

[82] N. M. Stall, W. Wu, L. Lapointe-Shaw, D. Fisman, M. Hillmer, and P. A. Rochon, "Sex-specific differences in COVID-19 testing, cases and outcomes: a population-wide study in Ontario, Canada," May 2020.

[83] K. L. Schwartz, C. Achonu, S. A. Buchan, K. A. Brown, B. Lee, M. Whelan, J. H. Wu, and G. Garber, "COVID-19 infections among healthcare workers and transmission within households," June 2020.

[84] N. G. Davies, P. Klepac, Y. Liu, K. Prem, M. Jit, and R. M. Eggo, "Age-dependent effects in the transmission and control of COVID-19 epidemics," *Nature medicine*, vol. 26, no. 8, pp. 1205–1211, 2020.

[85] J. Mossong, N. Hens, M. Jit, P. Beutels, K. Auranen, R. Mikolajczyk, M. Massari, S. Salmaso, G. S. Tomba, J. Wallinga, *et al.*, "Social contacts and mixing patterns relevant to the spread of infectious diseases," *PLoS Med*, vol. 5, no. 3, p. e74, 2008.

[86] K. Prem, A. R. Cook, and M. Jit, "Projecting social contact matrices in 152 countries using contact surveys and demographic data," *PLoS computational biology*, vol. 13, no. 9, p. e1005697, 2017.

[87] Government of Ontario, "Reopening Ontario," 2020.

[88] J. Zhang, M. Litvinova, Y. Liang, Y. Wang, W. Wang, S. Zhao, Q. Wu, S. Merler, C. Viboud, A. Vespignani, *et al.*, "Changes in contact patterns shape the dynamics of the COVID-19 outbreak in China," *Science*, vol. 368, no. 6498, pp. 1481–1486, 2020.

[89] M. U. Kraemer, C.-H. Yang, B. Gutierrez, C.-H. Wu, B. Klein, D. M. Pigott, L. Du Plessis, N. R. Faria, R. Li, W. P. Hanage, *et al.*, "The effect of human mobility and control measures on the COVID-19 epidemic in China," *Science*, vol. 368, no. 6490, pp. 493–497, 2020.

[90] M. Chinazzi, J. T. Davis, M. Ajelli, C. Gioannini, M. Litvinova, S. Merler, A. P. y Piontti, K. Mu, L. Rossi, K. Sun, *et al.*, "The effect of travel restrictions on the spread of the 2019 novel coronavirus (COVID-19) outbreak," *Science*, vol. 368, no. 6489, pp. 395–400, 2020.

[91] S. K. Ram and D. Sornette, "Impact of governmental interventions on epidemic progression and workplace activity during the COVID-19 outbreak," June 2020.

[92] D. Duque, D. P. Morton, B. Singh, Z. Du, R. Pasco, and L. A. Meyers, "COVID-19: How to relax social distancing if you must," May 2020.

[93] T. VoPham, M. D. Weaver, J. E. Hart, M. Ton, E. White, and P. A. Newcomb, "Effect of social distancing on COVID-19 incidence and mortality in the US," June 2020.

[94] R. Abouk and B. Heydari, "The immediate effect of COVID-19 policies on social distancing behavior in the United States," *SSRN Electronic Journal*, 2020.

[95] S. C. Anderson, A. M. Edwards, M. Yerlanov, N. Mulberry, J. Stockdale, S. A. Iyaniwura, R. C. Falcao, M. C. Otterstatter, M. A. Irvine, N. Z. Janjua, D. Coombs, and C. Colijn, "Estimating the impact of COVID-19 control measures using a Bayesian model of physical distancing," Apr. 2020.

[96] L. D. Domenico, G. Pullano, C. E. Sabbatini, P.-Y. Boëlle, and V. Colizza, "Expected impact of lockdown in île-de-france and possible exit strategies," Apr. 2020.

[97] C. I. Jarvis, K. V. Zandvoort, A. Gimma, K. Prem, P. Klepac, G. J. Rubin, and W. J. E. and, "Quantifying the impact of physical distance measures on the transmission of COVID-19 in the UK," Apr. 2020.

[98] J. Mossong, M. Jit, N. HENS, P. Beutels, K. Auranen, R. Mikolajczyk, M. Massari, G. Scalia-Tomba, J. Wallinga, M. Sadkowska-Todys, *et al.*, "Social contact and mixing patterns relevant to the spread of infectious diseases: a multi-country population-based survey," OXFORD UNIV PRESS, 2007.

[99] W. Lyra, J. D. do Nascimento, J. Belkhiria, L. de Almeida, P. P. Chrispim, and I. de Andrade, "Covid-19 pandemics modeling with SEIR (+ CAQH), social distancing, and age stratification. the effect of vertical confinement and release in Brazil," *medRxiv*, 2020.

[100] A. Radulescu and K. Cavanagh, "Management strategies in a SEIR model of COVID 19 community spread," *arXiv preprint arXiv:2003.11150*, 2020.

[101] R. voor Volksgezondheid en Milieu, "Children and COVID-19," 2020.

[102] Public Health Ontario, "Ontario covid-19 data tool," 2021.

[103] L. Humphrey, E. W. Thommes, R. Fields, N. Hakim, A. Chit, and M. G. Cojocaru, "A path out of covid-19 quarantine: an analysis of policy scenarios," *medRxiv*, 2020.

[104] F. Brauer, "The Kermack–McKendrick epidemic model revisited," *Mathematical biosciences*, vol. 198, no. 2, pp. 119–131, 2005.

[105] Government of Ontario, "News release: Ontario enacts declaration of emergency to protect the public," 2020.

[106] K. Mizumoto, K. Kagaya, A. Zarebski, and G. Chowell, "Estimating the asymptomatic proportion of coronavirus disease 2019 (COVID-19) cases on board the Diamond Princess cruise ship, Yokohama, Japan, 2020," *Eurosurveillance*, vol. 25, Mar. 2020.

[107] W. He, G. Y. Yi, and Y. Zhu, "Estimation of the basic reproduction number, average incubation time, asymptomatic infection rate, and case fatality rate for COVID-19: Meta-analysis and sensitivity analysis," *Journal of Medical Virology*, June 2020.

[108] Statistics Canada, "Table 17-10-0005-01. population estimates on July 1st, by age and sex," 2017.

[109] J. A. Backer, D. Klinkenberg, and J. Wallinga, "Incubation period of 2019 novel coronavirus (2019-ncov) infections among travellers from Wuhan, China, 20–28 january 2020," *Eurosurveillance*, vol. 25, no. 5, p. 2000062, 2020.

[110] J. Legrand, R. F. Grais, P.-Y. Boelle, A.-J. Valleron, and A. Flahault, "Understanding the dynamics of Ebola epidemics," *Epidemiology & Infection*, vol. 135, no. 4, pp. 610–621, 2007.

[111] L. Fumanelli, M. Ajelli, P. Manfredi, A. Vespignani, and S. Merler, "Inferring the structure of social contacts from demographic data in the analysis of infectious diseases spread," *PLoS computational biology*, vol. 8, no. 9, 2012.

[112] Z. R. Ravanera and R. Fernando, "Integration at late life: Inclusion, participation, and belonging among the elderly," *PSC Discussion Papers Series*, vol. 15, no. 16, p. 1, 2001.

[113] P. Arriagada, "A day in the life: How do older Canadians spend their time?," 2018.

[114] CDC COVID-19 Response Team, "Severe outcomes among patients with coronavirus disease 2019 (COVID-19)—United States, february 12–march 16, 2020," *MMWR Morb Mortal Wkly Rep*, vol. 69, no. 12, pp. 343–346, 2020.

[115] E. Abdollahi, M. Haworth-Brockman, Y. Keynan, J. M. Langley, and S. M. Moghadas, "Simulating the effect of school closure during COVID-19 outbreaks in Ontario, Canada," *BMC medicine*, vol. 18, no. 1, pp. 1–8, 2020.

[116] J. Wu, B. Tang, N. L. Bragazzi, K. Nah, and Z. McCarthy, "Quantifying the role of social distancing, personal protection and case detection in mitigating COVID-19 outbreak in Ontario, Canada," *Journal of Mathematics in Industry*, vol. 10, no. 1, pp. 1–12, 2020.

[117] D. Luenberger, *Linear and nonlinear programming*. New York: Springer, 2008.

[118] Ontario Agency for Health Protection and Promotion (Public Health Ontario), "Covid-19 in long-term care homes in Ontario: January 15, 2020 to February 28, 2021," 2021.

[119] W. Li, B. Zhang, J. Lu, S. Liu, Z. Chang, C. Peng, X. Liu, P. Zhang, Y. Ling, K. Tao, *et al.*, "Characteristics of household transmission of COVID-19," *Clinical Infectious Diseases*, vol. 71, no. 8, pp. 1943–1946, 2020.

[120] K. Yuki, M. Fujiogi, and S. Koutsogiannaki, "Covid-19 pathophysiology: A review," *Clinical immunology*, p. 108427, 2020.

[121] X. Lu, L. Zhang, H. Du, J. Zhang, Y. Y. Li, J. Qu, W. Zhang, Y. Wang, S. Bao, Y. Li, *et al.*, "Sars-cov-2 infection in children," *New England Journal of Medicine*, vol. 382, no. 17, pp. 1663–1665, 2020.

[122] W. Gardner, D. States, and N. Bagley, "The coronavirus and the risks to the elderly in long-term care," *Journal of Aging & Social Policy*, pp. 1–6, 2020.

[123] Statistics Canada, "Table 17100005 population estimates on July 1st, by age and sex, annually, series v466935, v468810, v468813, v468816, v468819, v468822, v468825," 2021.

APPENDICES

Appendix A

Supplementary data for shingles distribution model

A.1 Population estimates

Table A.1: Population numbers for 65-69 year olds from 2016-2020, taken from yearly provincial estimates [123].

G_i	$N_i(2016)$	$N_i(2017)$	$N_i(2018)$	$N_i(2019)$	$N_i(2020)$
G_1: 65-66	152,930	156,367	162,441	169,071	176,043
G_2: 66-67	148,584	151,966	155,275	161,297	167,620
G_3: 67-68	145,840	147,573	150,753	154,157	159,862
G_4: 68-69	146,319	144,607	146,197	149,508	152,632
G_5: 69-70	146,037	144,905	143,127	144,968	147,805

A.2 Age group-specific distribution results

Table A.2: Population numbers for 65-69 year olds in 2021-2024 are projections from 2020 population estimates for 61-64 year olds using average Ontario growth rate trends for seniors from the last decade [123].

G_i	$N_i(2020)$	$N_i(2021)$	$N_i(2022)$	$N_i(2023)$	$N_i(2024)$
G_1: 65-66	176,043	179,184	185,585	189,543	193,397
G_2: 66-67	167,620	175,118	178,536	184,952	188,602
G_3: 67-68	159,862	166,534	174,198	177,890	184,321
G_4: 68-69	152,632	158,774	165,455	173,282	177,246
G_5: 69-70	147,805	151,607	157,693	164,383	172,372

Table A.3: Model results for doses administered and effective coverage with Zostavax in 2020 by age.

Age	Doses (% of group)	Coverage (% of group)
65	8.09	5.18
66	25.43	13.86
67	57.27	24.92
68	88.99	34.79
69	96.22	36.93
70	88.684	32.03
71	70.99	23.18
72	39.21	12.21
73	11.81	3.60

Table A.4: Model results for doses administered and effective coverage with Shingrix in 2024 by age.

Age	Doses (% of group)	Coverage (% of group)
65	0	0
66	1.58	1.54
67	31.25	28.75
68	63.08	56.46
69	68.48	61.05
70	70.29	62.77
71	68.63	61.18
72	37.41	32.43
73	5.75	4.89

Appendix B

Supplementary calculations for SEILR(pas) model

B.1 Collapsing age-stratified contact matrices

In [86] (a study of country-specific contact rates), a 16x16 contact matrix provides contact rates between Canadians aged $0-80$ in 5-year intervals with the each row representing the age interval of an individual, and the age interval of the group being contacted listed on the columns. The highly stratified contact rates in this 16x16 matrix were then combined to create a condensed 3x3 contact matrix in accordance to our selected age groups in the following manner:

1. Columns are partitioned into the three age groups with which individuals come into contact: Group 1 (0-19), Group 2 (20-59), and Group 3 (60-80[asterisk]*).

2. Contacts are summed in each row in accordance with the new column partitions, yielding a 16x3 matrix, representing each of the 16 age groups' combined contacts with each of the 3 new age groups created

3. A population-weighted average of each respective cumulative contact-rate for all members of each group was taken to generate our final 3x3 matrix in accordance with our new age groups, outlined below. Each interval's population was taken from [108].

B.2 Initial start date

We choose to begin our model on February 14, after which iPHIS reports only a single day with zero new cases. While Ontario's official declaration of emergency was on March 17, 2020, we chose an earlier date for our simulated model due to the fact that March 17 is mid-work week. The majority of contacts occur in the workplace or in educational facilities. Since most workplaces and educational facilities close for the weekend, and educational facilities of all levels announced COVID-19-related closures on Friday March 13th at the latest, contact mitigation effectively began on Monday March 16th (or earlier).

B.3 Matching the delay between simulated data and iPHIS data

In theory, individuals should wait through the incubation period from time of exposure before displaying symptoms and becoming a member of I^S_{new} (3.5 days in E, 2.5 days in I^P, 6 days total). Unfortunately, the terms representing time in SEIR models (σ, ψ, κ, and γ) do not actually function as delayers, but rather dampeners. For instance $\sigma = 1/2.5$ should represent a 2.5 day latency period, and so individuals should have to wait 2.5 days from time of exposure before entering I^P, however the equation

$$I^P_{new}(t) = \sum_{i=1}^{3} \sigma \cdot E_i(t-1)$$

shows that $\sigma = 1/2.5$ of members of E will enter I^P on the very first day after entering E. Similarly, with the equation

$$I^S_{new}(t) = \sum_{i=1}^{3} \alpha \cdot \psi \cdot I^P_i(t-1)$$

we can see that $\psi \cdot \alpha = 1/2 \cdot 1/3.5 = 1/7$ of those in I^P will enter I^S on the first day after entering I^P. As a result, $\psi \cdot \alpha \cdot \sigma = 1/17.5$ of people exposed on day t will enter I^S on day $t+2$, with the remainder through the days following. With this in mind, we must introduce a delay term of at least 2-6 days from when we change q to when we match I^S_{new} with Ontario iPHIS data. This means that when finding the optimal value of q from day t to day $t+7$, we compare I^S_{new} with Ontario iPHIS on days $t + delay$ to day $t + delay + 7$, since a change in q will not result in a change I^S_{new} for $delay$ days. After testing delay terms of 0-7, and initial intervention dates from March 12 -March 17, we found an optimal combination of a 2 day matching delay with an initial intervention date of March 15 to minimize our SSE (see Figure B.1).

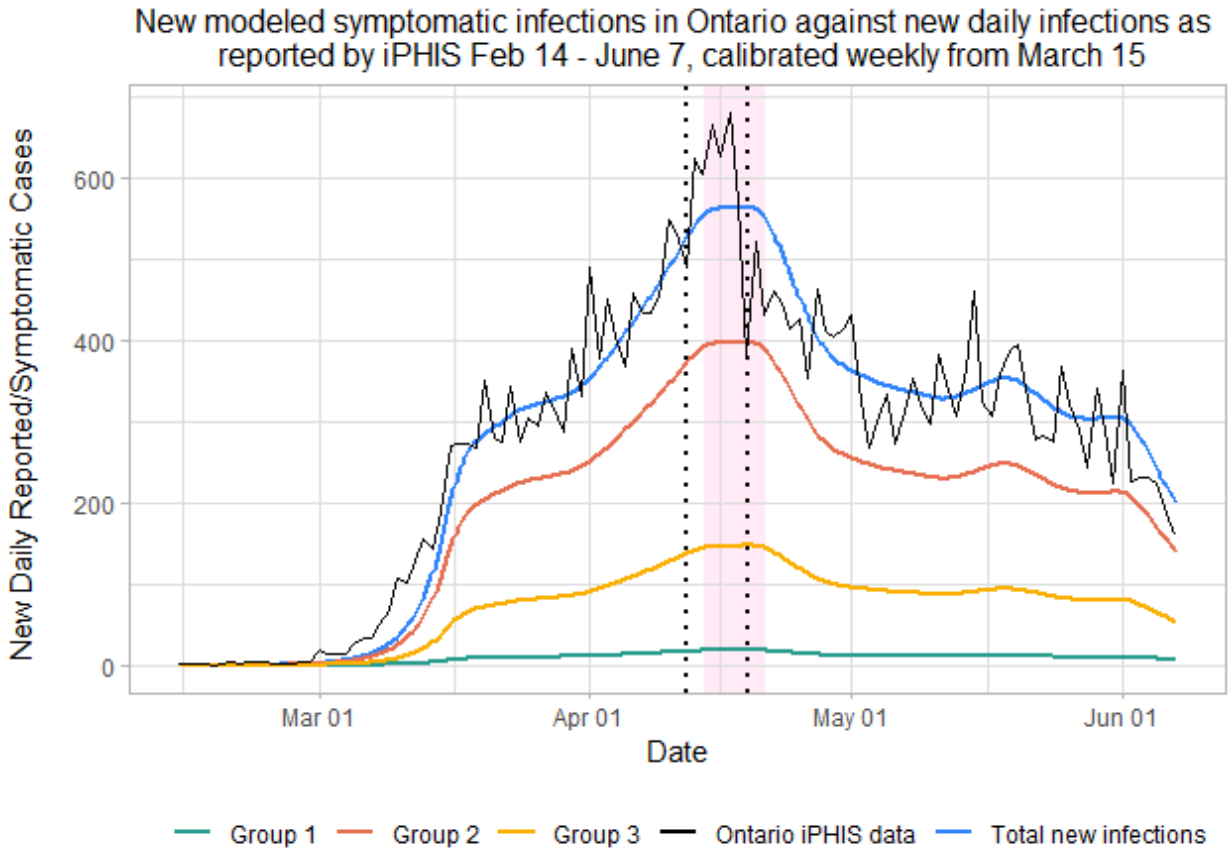

Figure B.1: To solve for the q value for time interval int (between the two black lines), we find the SSE during time interval $int + 2$ (red shaded region).